

RESEARCH

Open Access



Therapeutic potential of berberine in attenuating cholestatic liver injury: insights from a PSC mouse model

Yanyan Wang^{1,2}, Derrick Zhao¹, Lianyong Su¹, Yun-Ling Tai¹, Grayson W. Way¹, Jing Zeng¹, Qianhua Yan^{1,3}, Ying Xu¹, Xuan Wang¹, Emily C. Gurley¹, Xi-Qiao Zhou³, Jinze Liu⁴, Jinpeng Liu⁵, Weidong Chen², Phillip B. Hylemon¹ and Huiping Zhou^{1*} 

Abstract

Background and aims Primary sclerosing cholangitis (PSC) is a chronic liver disease characterized by progressive biliary inflammation and bile duct injury. Berberine (BBR) is a bioactive isoquinoline alkaloid found in various herbs and has multiple beneficial effects on metabolic and inflammatory diseases, including liver diseases. This study aimed to examine the therapeutic effect of BBR on cholestatic liver injury in a PSC mouse model (*Mdr2*^{-/-} mice) and elucidate the underlying mechanisms.

Methods *Mdr2*^{-/-} mice (12–14 weeks old, both sexes) received either BBR (50 mg/kg) or control solution daily for eight weeks via oral gavage. Histological and serum biochemical analyses were used to assess fibrotic liver injury severity. Total RNAseq and pathway analyses were used to identify the potential signaling pathways modulated by BBR in the liver. The expression levels of key genes involved in regulating hepatic fibrosis, bile duct proliferation, inflammation, and bile acid metabolism were validated by qRT-PCR or Western blot analysis. The bile acid composition and levels in the serum, liver, small intestine, and feces and tissue distribution of BBR were measured by LC–MS/MS. Intestinal inflammation and injury were assessed by gene expression profiling and histological analysis. The impact on the gut microbiome was assessed using 16S rRNA gene sequencing.

Results BBR treatment significantly ameliorated cholestatic liver injury, evidenced by decreased serum levels of AST, ALT, and ALP, and reduced bile duct proliferation and hepatic fibrosis, as shown by H&E, Picro-Sirius Red, and CK19 IHC staining. RNAseq and qRT-PCR analyses indicated a substantial inhibition of fibrotic and inflammatory gene expression. BBR also mitigated ER stress by downregulating Chop, Atf4 and Xbp-1 expression. In addition, BBR modulated bile acid metabolism by altering key gene expressions in the liver and small intestine, resulting in restored bile acid homeostasis characterized by reduced total bile acids in serum, liver, and small intestine and increased fecal excretion. Furthermore, BBR significantly improved intestinal barrier function and reduced bacterial translocation by modulating the gut microbiota.

Conclusion BBR effectively attenuates cholestatic liver injury, suggesting its potential as a therapeutic agent for PSC and other cholestatic liver diseases.

Keywords Bile acids, Cholestasis, Inflammation, Berberine, Gut microbiome

*Correspondence:

Huiping Zhou

huiping.zhou@vcuhealth.org; Huiping.zhou@va.gov

Full list of author information is available at the end of the article



This is a U.S. Government work and not under copyright protection in the US; foreign copyright protection may apply 2024. **Open Access** This article is licensed under a Creative Commons Attribution 4.0 International License, which permits use, sharing, adaptation, distribution and reproduction in any medium or format, as long as you give appropriate credit to the original author(s) and the source, provide a link to the Creative Commons licence, and indicate if changes were made. The images or other third party material in this article are included in the article's Creative Commons licence, unless indicated otherwise in a credit line to the material. If material is not included in the article's Creative Commons licence and your intended use is not permitted by statutory regulation or exceeds the permitted use, you will need to obtain permission directly from the copyright holder. To view a copy of this licence, visit <http://creativecommons.org/licenses/by/4.0/>. The Creative Commons Public Domain Dedication waiver (<http://creativecommons.org/publicdomain/zero/1.0/>) applies to the data made available in this article, unless otherwise stated in a credit line to the data.

Background

Primary sclerosing cholangitis (PSC) is a chronic cholestatic liver disorder characterized by inflammation and bile duct narrowing, which results in the accumulation of bile acids (BAs) in the liver, leading to hepatic damage, progressive liver fibrosis, cirrhosis, and even liver cancer [1, 2]. Over the last several decades, extensive efforts have been made to identify the mechanisms underlying cholestatic liver injury [3–5]. However, no effective therapy has been developed due to the complexity of disease pathogenesis. Liver transplantation remains the only life-extending treatment for end-stage PSC patients [4]. It has been well-accepted that dysregulation of BA homeostasis and inflammation are the major driving forces of the disease progression of PSC [6]. In addition, dysbiosis and intestinal barrier dysfunction also have been reported as key contributors to cholestatic liver injury [7–9]. Therefore, an effective therapeutic agent for PSC must be able to modulate bile acid metabolism, inflammatory response, and the gut microbiome.

Berberine (BBR), an isoquinoline alkaloid isolated from the rhizome of the herb *Coptis chinensis* and *Berberis vulgaris*, is one of the most commonly used plant medicines in China and Asia with various biological activities [10–13]. BBR has been reported as a promising therapeutic agent for cardiovascular and metabolic diseases, including metabolic dysfunction associated fatty liver disease (MAFLD) and diabetes [10, 14–17]. BBR's beneficial effect on hepatic lipid homeostasis is achieved via regulating BA synthesis and excretion [15]. We have previously reported that BBR can inhibit HIV protease inhibitor-induced ER stress in macrophages and inhibit free fatty acid and LPS-induced inflammation via modulating ER stress response in macrophages and hepatocytes [17, 18]. Our recent study further showed that BBR could not only inhibit hepatic fibrosis by modulating the expression of multiple genes involved in hepatic stellate cell activation and cholangiocyte proliferation but also restore the BA homeostasis in the diet-induced metabolic dysfunction-associated steatohepatitis (MASH) mouse model [16]. However, the therapeutic effect of BBR on cholestatic liver disease has not been studied and is the primary focus of this study.

The current study tested the therapeutic effect of BBR on the cholestatic liver disease and further examined the potential cellular/molecular mechanisms using the best available PSC mouse model, *Mdr2*^{-/-} mice [19–21]. The results indicated that BBR significantly reduced cholestatic liver injury via modulating BA metabolism and gut microbiota, inhibiting the inflammatory response and ER stress and protecting intestinal barrier function.

Results

BBR improves cholestatic liver injury in *Mdr2*^{-/-} mice

Mdr2^{-/-} mice are a well-established model of cholestatic cholangiopathies [19–21]. To examine the therapeutic effect of BBR on cholestatic liver injury, *Mdr2*^{-/-} mice (FVB background, 12–14 weeks old) were treated with BBR (50 mg/kg) or vehicle by intragastric administration once daily for 8 weeks. As shown in Figs. 1a–b, BBR significantly reduced the ratio of liver weight to body weight compared to the control *Mdr2*^{-/-} mice. The serum alkaline phosphatase (ALP), aspartate aminotransferase (AST) and alanine aminotransferase (ALT) levels were also significantly reduced by BBR in *Mdr2*^{-/-} mice (Fig. 1c). The body weight and total serum albumin (ALB) levels remained unchanged (Additional file 1: Fig. S1a, b). Histological analysis showed that BBR treatment significantly reduced cholestatic liver injury as illustrated by H&E staining (Fig. 1d). To further verify the therapeutic effect of BBR on cholestatic liver injury, we did the same study using *Mdr2*^{-/-} mice with C57BL/6 background. As shown in Additional file 1: Fig. S1c, d, similar results were obtained. BBR treatment not only reduced the serum levels of AST, ALT, and ALP, but also reduced cholestatic liver injury as indicated by H&E staining.

BBR reduces cholestatic liver injury by modulating global transcriptomic profile in *Mdr2*^{-/-} mice

To examine the underlying mechanisms by which BBR reduces cholestatic liver injury in *Mdr2*^{-/-} mice, total RNA transcriptome analysis was performed. As shown in Additional file 1: Fig. S2a, the heatmap showed distinct expression profiles between the WT and *Mdr2*^{-/-} mice, while the BBR treatment group showed a similar profile to the WT mice. The volcano plot further showed the change of gene expression induced in *Mdr2*^{-/-} mice was significantly reversed by BBR treatment (Figs. 2b and Additional file 1: Fig. S2b). As shown in Additional file 1: Fig. S2c, compared to the WT mice, the *Mdr2*^{-/-} mice exhibited an upregulation of 1260 genes and down-regulation of 677 genes, while BBR treatment down-regulated 287 genes and upregulated 300 genes, compared to vehicle-treated *Mdr2*^{-/-} mice. Furthermore, Gene Ontology analysis and Kyoto Encyclopedia of Genes and Genomes (KEGG) pathways analysis showed that BBR was able to impact the pathways in biological process, cellular components, and molecular function, such as regulation of transcription, cellular response to fibroblast growth factor stimulus, extracellular matrix, endoplasmic reticulum, etc. (Figs. 2c–f). IPA (Ingenuity Pathway Analysis) further showed that the hepatic fibrosis signaling pathway, tumor microenvironment pathway, IL-17 signaling, HER-2 signaling and GHRH signaling were activated in *Mdr2*^{-/-} mice, which were inhibited after BBR treatment

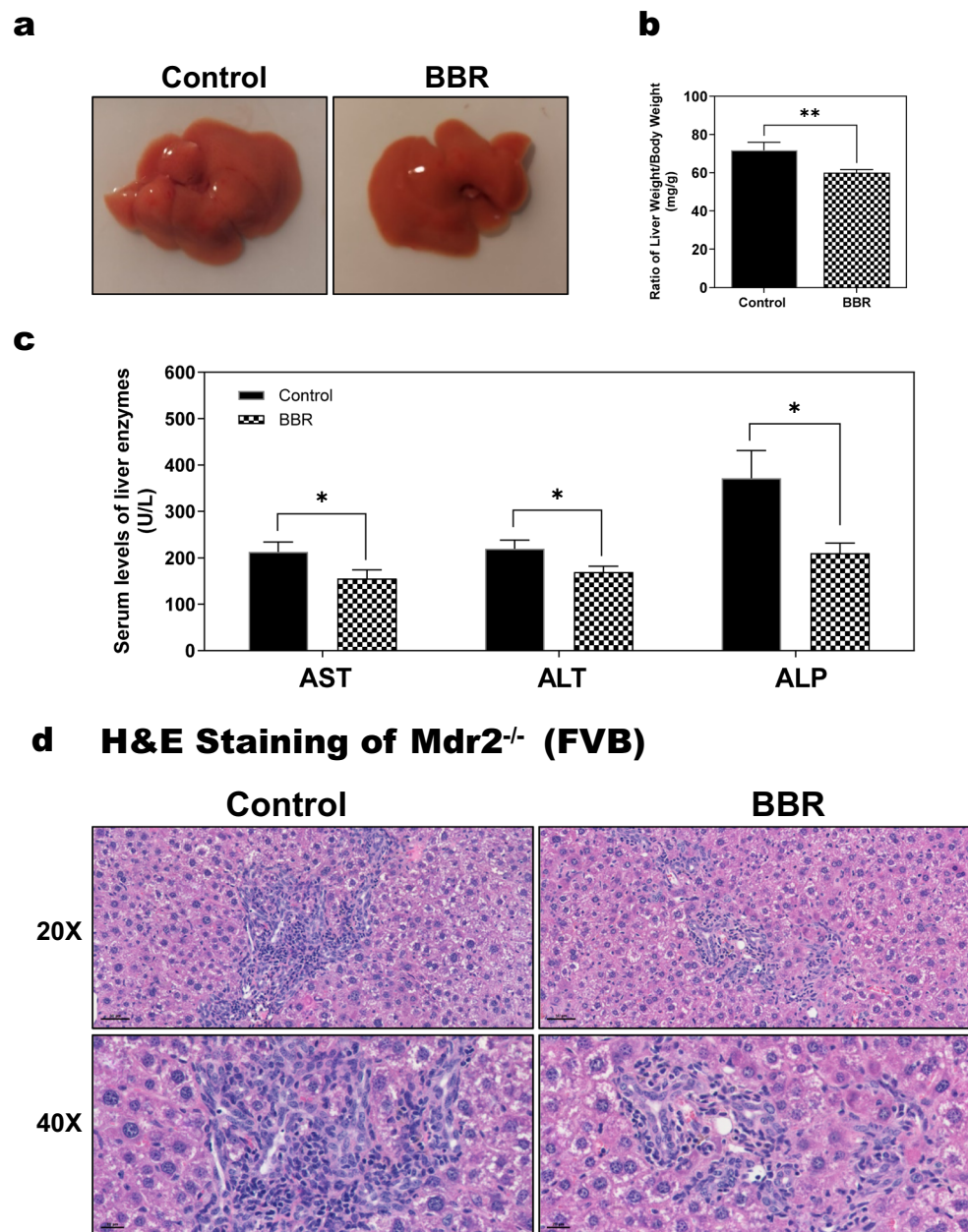


Fig. 1 Effect of BBR on cholestatic liver injury in Mdr2^{-/-} mice. Mdr2^{-/-} mice (FVB background, both sexes) were treated with vehicle (Control group) or BBR (50 mg/kg) (BBR group) via oral gavage daily for 8 weeks. **a** Representative liver images. **b** The ratio of liver weight to body weight. **c** Serum liver enzyme levels (AST, ALT, ALP). **d** Representative images of the liver sections stained with H&E staining (scale bar, 50 μ m for 20 \times , 20 μ m for 40 \times magnification). Data are expressed as the mean \pm SEM. Statistical significance relative to control: * p < 0.05, ** p < 0.01 (n = 9–12)

(Additional file 1: Fig. S3). In addition, the activated senescence pathway was also inhibited by BBR.

BBR attenuates bile duct injury and hepatic fibrosis in Mdr2^{-/-} mice

The proliferation of bile ducts and hepatic fibrosis are associated with the development of cholestatic liver injury [22]. Picro-Sirius Red staining of the liver

tissue sections showed that BBR treatment significantly reduced hepatic fibrosis in Mdr2^{-/-} mice, as shown in Figs. 3a-b. Importantly, BBR treatment significantly decreased proliferation of bile ducts as determined by IHC staining of keratin 19 (Krt19, also known as Ck19) and Ki67 (Figs. 3c-f and Additional file 1: Fig. S4a). In addition, BBR treatment significantly decreased the content of hepatic hydroxyproline in Mdr2^{-/-} mice

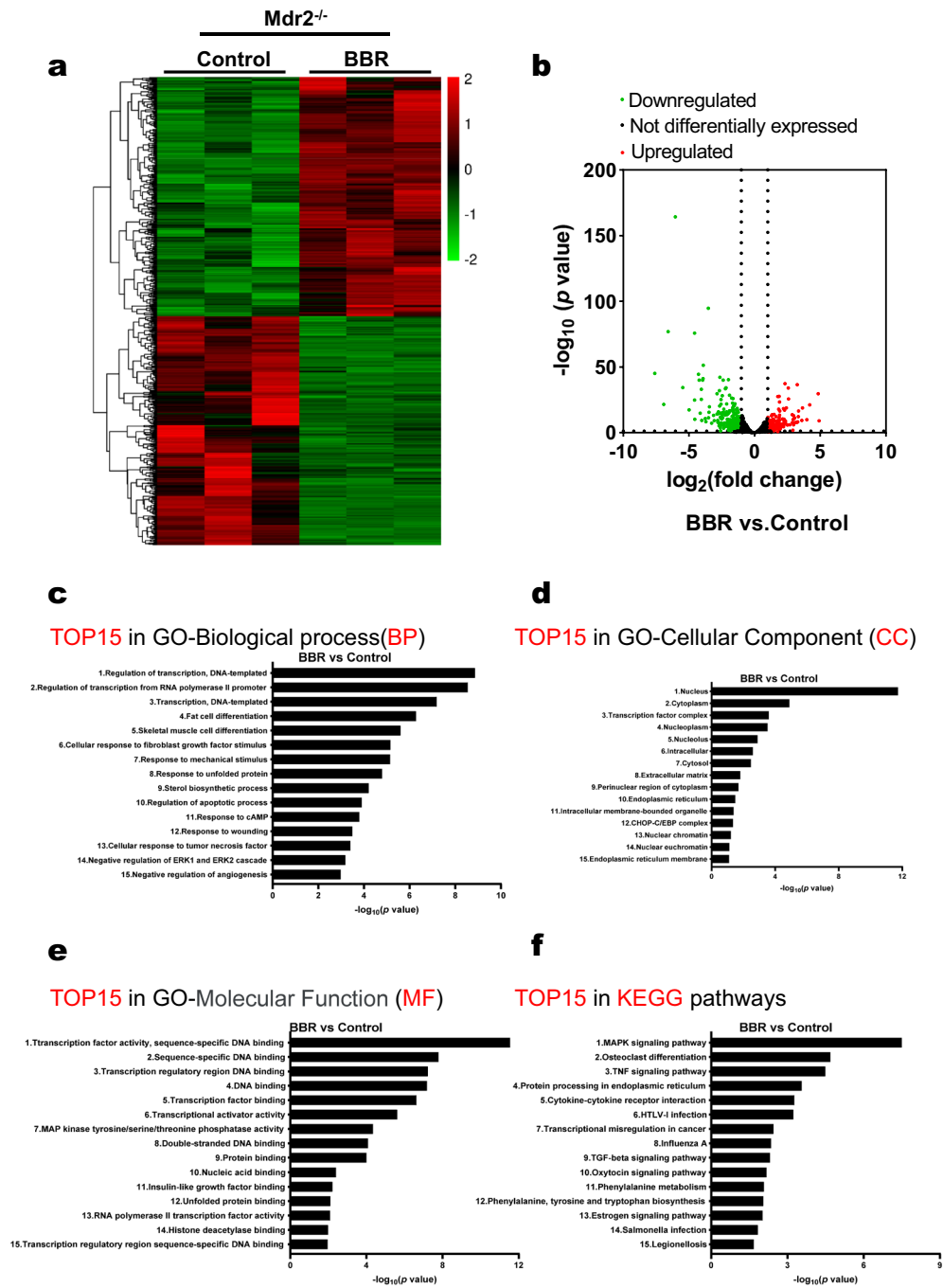


Fig. 2 Transcriptomic Profiling and Pathway Analysis of Differentially Expressed Genes (DEGs) in BBR-treated *Mdr2^{-/-}* mice. Liver RNA samples from each experimental group (three per group) underwent total transcriptome sequencing (RNA-seq). DEGs between the BBR-treated and control groups were identified using fold change (FC) and p-values (FC ≥ 2 and p-value < 0.05). Subsequent Gene Ontology and Kyoto Encyclopedia of Genes and Genomes (KEGG) pathway analyses were conducted. **a** Hierarchical clustering heatmaps display DEGs, with a Z-score normalization of RNA-seq data. Red and green colors signify up- and down-regulated gene expression, respectively. **b** Volcano plots show gene expression differences; red dots represent upregulated genes, green dots for downregulated genes, and black dots for genes not differentially expressed. **c** Top 15 enriched biological processes (GO-BP), **d** cellular components (GO-CC), and **e** molecular functions (GO-MF). **f** Highlights the top 15 enriched pathways according to KEGG analysis

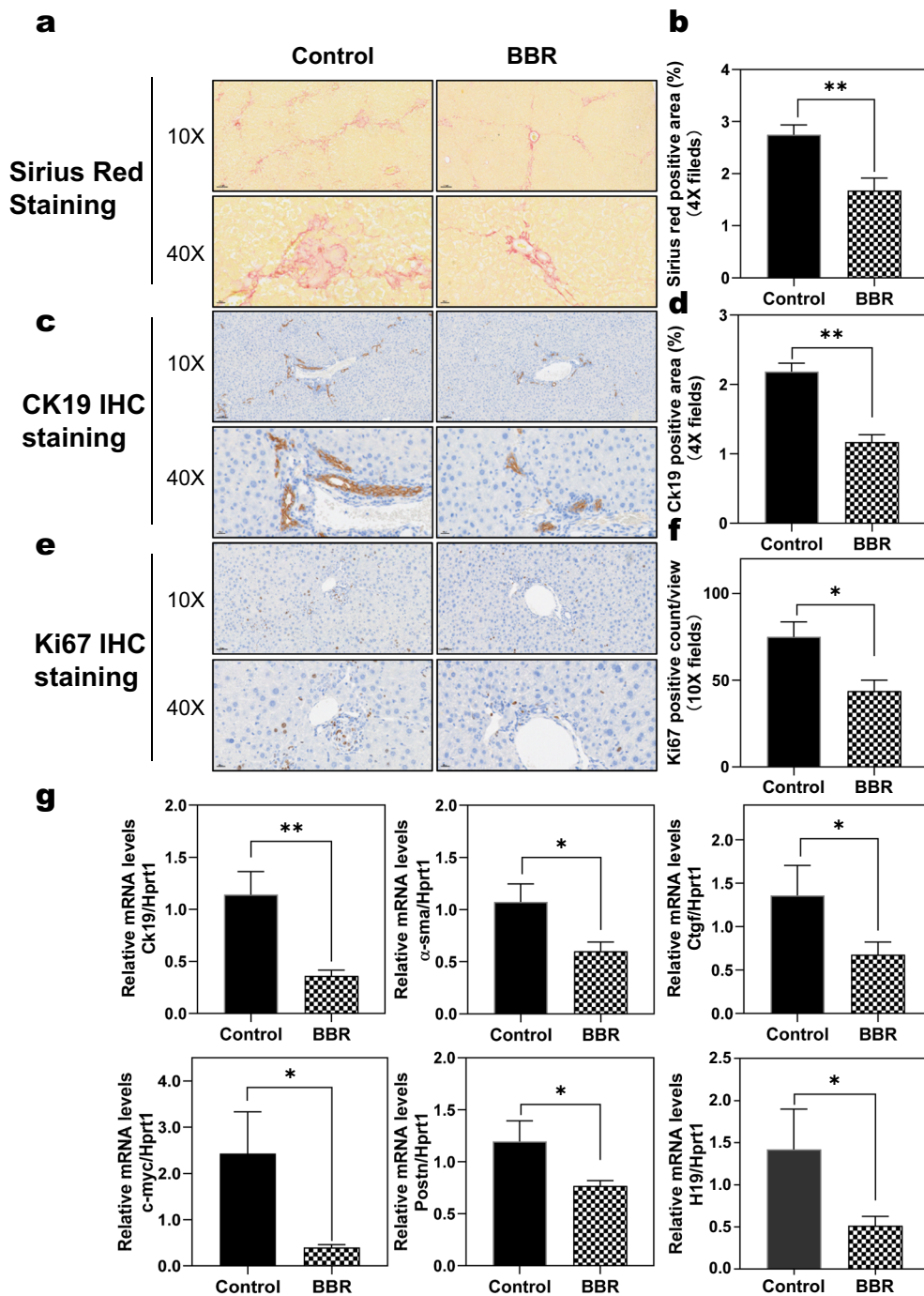


Fig. 3 Effect of BBR on ductular proliferation and cholestatic liver fibrosis in *Mdr2*^{-/-} mice. **a** Representative images of liver sections stained with Picro-Sirius Red (scale bar, 100 μ m for 10x and 20 μ m for 40x magnification). **b** Quantification of Sirius red staining. **c** Representative images of IHC staining of CK19 (cytokeratin 19). **d** Quantified positive area of CK19 staining. **e** Representative images of IHC staining of Ki67. **f** Quantification of Ki67 positive cells. **g** Relative mRNA levels of key genes involved in ductular proliferation and cholestatic liver fibrosis: Ck19, α -Sma, Ctgf, C-myc, Postn, and H19. The mRNA levels were determined by real-time RT-PCR and normalized with HPRT1 as an internal control. Data are expressed as the mean \pm SEM. Statistical significance relative to Control group is indicated as * p < 0.05, ** p < 0.01 (n = 9–12)

(Additional file 1: Fig. S4b). As shown in the Fig. 3g and Additional file 1: Fig. S5a, major fibrotic genes were significantly downregulated after BBR treatment in *Mdr2*^{-/-} mice, such as *Ck19*, α -Sma (smooth muscle actin), *Ctgf* (connective tissue growth factor), *C-myc* (cellular myelocytomatosis oncogene), *Postn* (periostin, osteoblast specific factor), etc. Although RNA-seq data did not identify significant changes in *H19* (long non coding RNA *H19*), the real-time RT-PCR analysis showed that BBR significantly reduced *H19* expression. Moreover, BBR was able to reduce the mRNA levels of *Pai1*, *Col12a1*, *Sox9*, *Egr1*, *Egr2*, *Egr3*, *Hbegf*, *Cyr61*, and *P4ha1* in *Mdr2*^{-/-} mice (Additional file 1: Fig. S5b).

BBR reduces hepatic inflammation and stress in *Mdr2*^{-/-} mice

Inflammation and oxidative stress response are key factors in cholestatic liver injury disease progression. The nuclear factor- κ B (NF- κ B) pathway is one of the main signaling pathways associated with inflammatory responses and plays a significant role in cholestatic liver disease progression [23]. As shown in Fig. 4a, b, Western blot analysis indicated that BBR treatment significantly reduced the activation of NF- κ B in *Mdr2*^{-/-} mice. The RNA-seq data also showed that BBR significantly inhibited the expression of key genes involved in hepatic inflammation and stress (Additional file 1: Fig. S6). We further confirmed the expression levels of chemokine (C-C motif) ligand 2 (*Ccl2/Mcp-1*), chemokine (C-C motif) receptor 2 (*Ccr2*), chemokine (C-X-C motif) ligand 1 (*Cxcl1*), interleukin (IL)-1 α , and IL-1 β , jun proto-oncogene (*Jun*), FBJ osteosarcoma oncogene (*Fos*), vascular cell adhesion molecule 1 (*Vcam-1*), *Cd86*, caspase 4, and *Cd83*, selectin (*Sell*) using the real-time RT-PCR. As shown in Fig. 4c, BBR treatment significantly reduced the expression of these inflammatory genes in *Mdr2*^{-/-} mice. In addition, as shown in Additional file 1: Figs. S7–S9, pathway analysis showed that BBR was able to inhibit the activation of NF- κ B signaling pathway, MAPK signaling pathway, and oxidative phosphorylation in *Mdr2*^{-/-} mice.

BBR modulates endoplasmic reticulum (ER) stress in *Mdr2*^{-/-} mice

Endoplasmic reticulum (ER) stress occurs when ER homeostasis is perturbed by the accumulation of unfolded/misfolded protein or calcium depletion [24]. Our previous studies and studies from others demonstrate a crucial role of ER stress in the development of liver fibrosis in cholestatic liver disease [7, 25]. As shown in Fig. 5a, the heatmap displayed a dramatic down-regulation of major genes in ER stress in *Mdr2*^{-/-} mice treated with BBR. To further confirm the findings of RNA-seq

analysis, we measured both mRNA and protein expression levels of key genes involved in ER stress. As shown in Fig. 5b, consistent with RNA-seq analysis, real-time RT-PCR showed that BBR significantly downregulated the mRNA expression level of CCAAT/enhancer-binding protein homologous protein (*Chop*), activating transcription factor 4 (*Atf4*), X-box binding protein 1 (*Xbp-1*), and dual specificity phosphatase 1 (*Dusp1*) in *Mdr2*^{-/-} mice. Similarly, the Western-blot analysis further showed that BBR decreased the protein expression levels of p-ERK/ERK, ATF4, and XBP-1s in *Mdr2*^{-/-} mice (Figs. 5c, e, and g). As shown in Figs. 5d, f, the nuclear protein expression of CHOP was significantly reduced by BBR treatment in *Mdr2*^{-/-} mice. Furthermore, as shown in Additional file 1: Fig. S10, pathway analysis showed that BBR was able to restore the dysregulation of protein processing in the ER in *Mdr2*^{-/-} mice.

BBR modifies the bile acid metabolism in *Mdr2*^{-/-} mice

Bile acid (BA) synthesis and transport are crucial for regulating the amount of BA in circulation [6]. As shown in Additional file 1: Fig. S11, the heatmap from RNA-seq analysis showed the key gene in primary bile acid biosynthesis, *Cyp7a1* (Cholesterol 7 α -hydroxylase), the rate-limiting enzyme in classical pathways of BA synthesis, was significantly increased by BBR treatment in *Mdr2*^{-/-} mice. BBR also modulated the expression of genes involved in hepatic transporters and nuclear receptors, such as *Abcg5*, *Asbt* (*Slc10a2*), *Shp*, farnesoid X receptor α (*Fxr α*), etc. To further confirm the results of RNA-seq data, we measured the expression of the major genes using real-time RT-PCR. As shown in Fig. 6a–c, BBR significantly increased the mRNA expression level of *Cyp7a1*, *Shp*, and *Fxr α* . Western-blot analysis further showed that the protein expression levels of CYP7A1, SHP, and FXR α were significantly increased in *Mdr2*^{-/-} mice treated with BBR (Fig. 6d–e). As shown in Fig. 6f, the mRNA expression level of *Cyp27a1*, *Cyp7b1*, and *Abcg5* were also increased in *Mdr2*^{-/-} mice by BBR, while the expression of *Asbt* and *Nr4a1* were decreased by BBR. Although RNA-seq data did not identify significant changes in *Ntcp* (*Slc10a1*), the real-time PCR analysis showed that BBR was able to reduce the expression of *Ntcp*.

BBR restores the BA homeostasis in *Mdr2*^{-/-} mice

Previous studies have reported that interruption of the enterohepatic circulation of BA protects against BA-mediated cholestatic liver and bile duct injury [26, 27]. Our recent study indicated that BBR restored the BA homeostasis in MASH mice [16]. To examine the effect of BBR on BA profile in *Mdr2*^{-/-} mice, we measured more than 30 different BAs in the serum, liver,

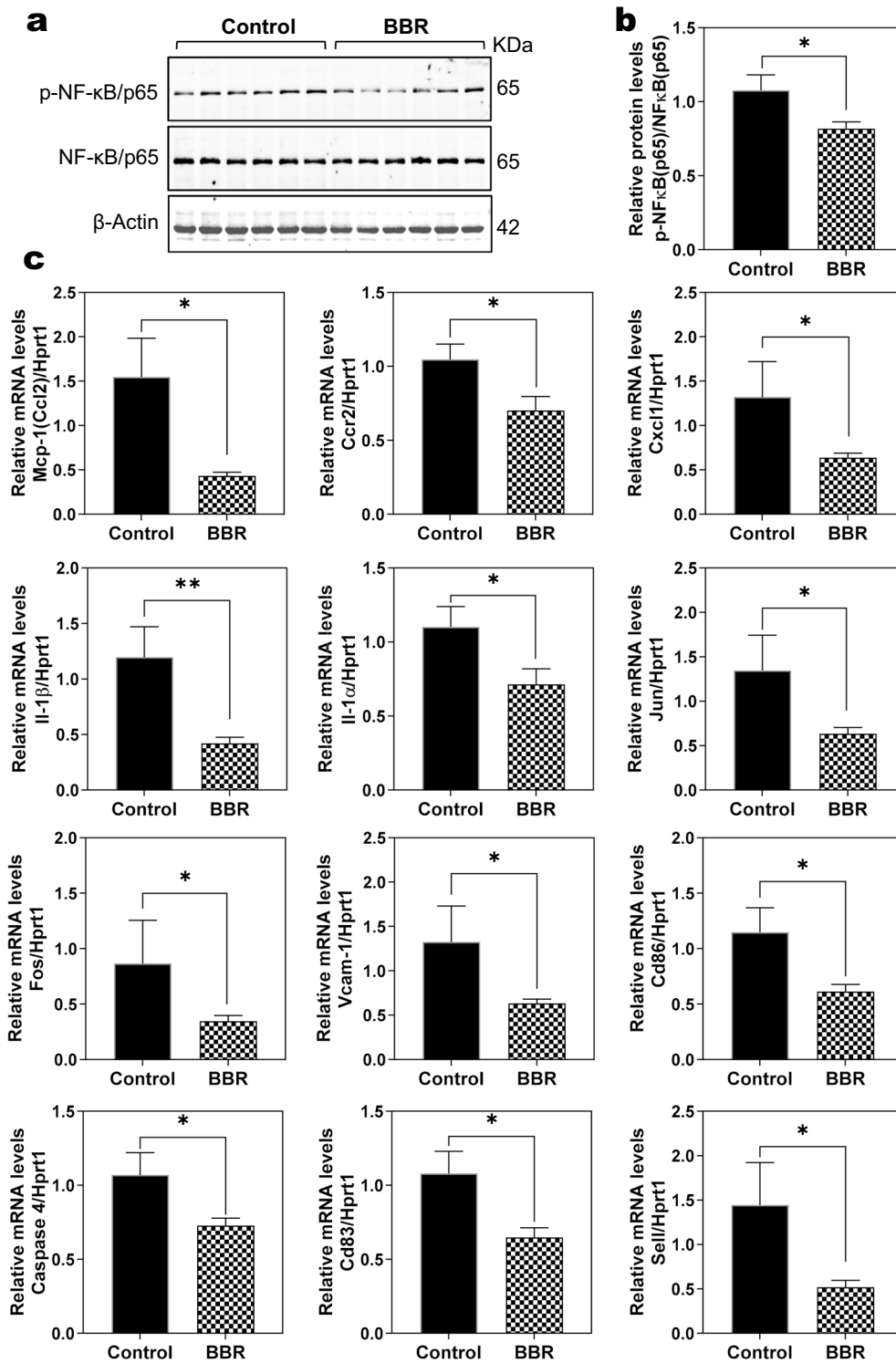


Fig. 4 Effect of BBR on hepatic inflammation in *Mdr2*^{-/-} mice. **a** Representative immunoblot images of phosphorylated (p)-nuclear factor (NF)-κB/p65, total NF-κB/p65, and loading control β-Actin are shown. **b** The relative protein level of p-NF-κB/p65, normalized to total NF-κB/p65. **c** Relative mRNA levels of inflammation-related genes implicated in cholestatic liver injury, including *Mcp-1(Ccl2)*, *Ccr2*, *Cxcl1*, *IL-1α*, *IL-1β*, *Jun*, *Fos*, *Vcam-1*, *Cd86*, *Casp 4*, *Cd83* and *Sell*, normalized with *HPRT1* as an internal control. Data are expressed as the mean ± SEM. Statistical significance relative to Control group: **p* < 0.05, ***p* < 0.01 (n = 9–12)

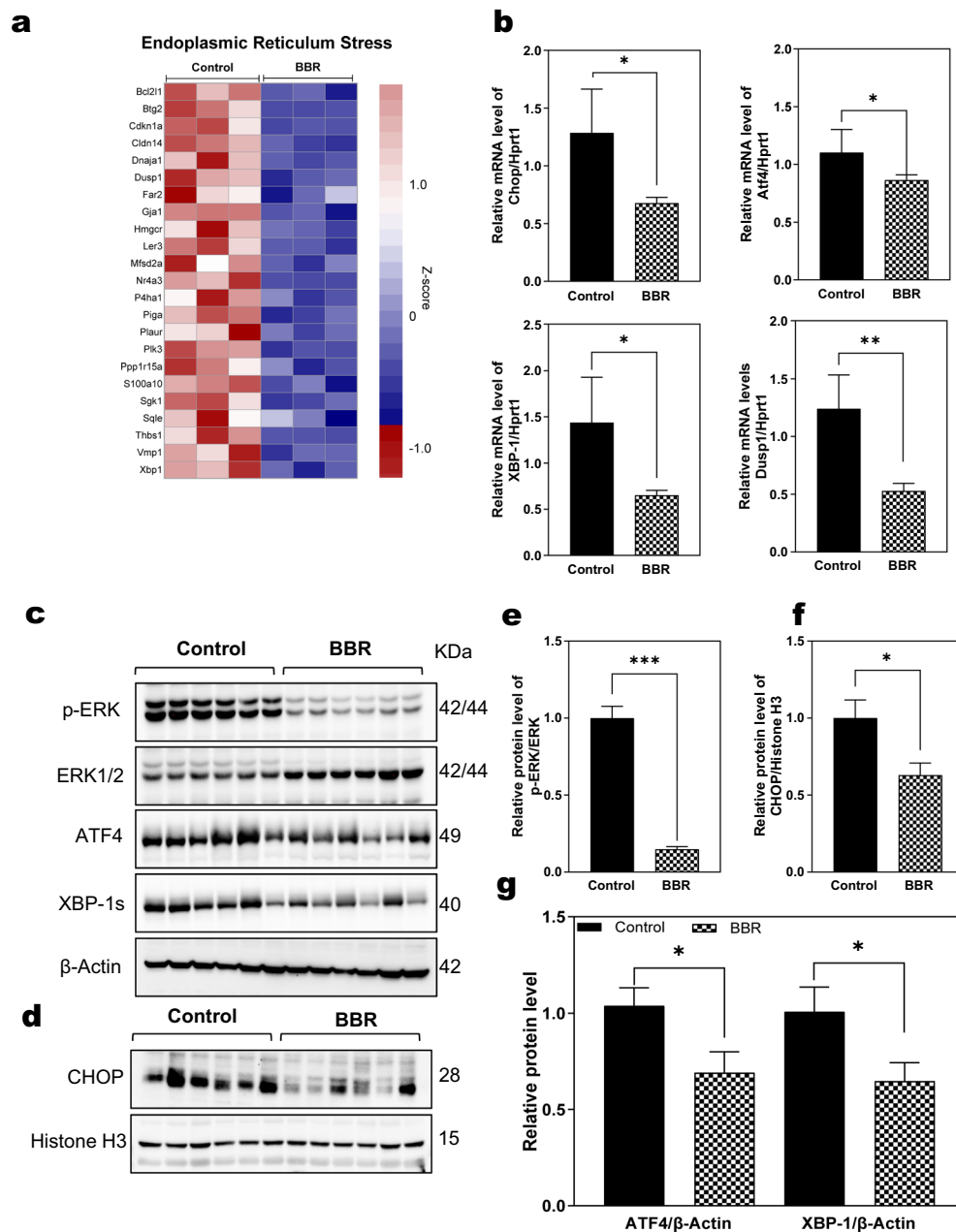


Fig. 5 Effect of BBR on hepatic endoplasmic reticulum (ER) stress in *Mdr2*^{-/-} mice. **a** Representative heatmap of the key genes involved in ER stress response in the liver, comparing BBR-treated group with the Control group. The RNA-seq data were normalized using a Z-score for tag counts, with red and blue colors denoting high and low gene expression, respectively. **b** Relative mRNA expression levels of ER stress-related genes (Chop, Atf4, Xbp-1, and Dusp1), normalized with HPRT1 as an internal control. **c** Representative immunoblot images of phosphorylated (p)-ERK, total ERK, ATF4, and XBP-1. **d** Representative immunoblot images of nuclear CHOP. **e** Relative protein level of p-ERK, normalized using ERK as a loading control. **f** Relative protein level of CHOP, normalized with Histone H3 as a loading control. **g** Relative protein levels of ATF4 and XBP-1, normalized against β -actin as a loading control. Data are expressed as mean \pm SEM. Statistical significance compared to the control group is indicated as * $p < 0.05$, ** $p < 0.01$, *** $p < 0.001$ ($n = 9-12$)

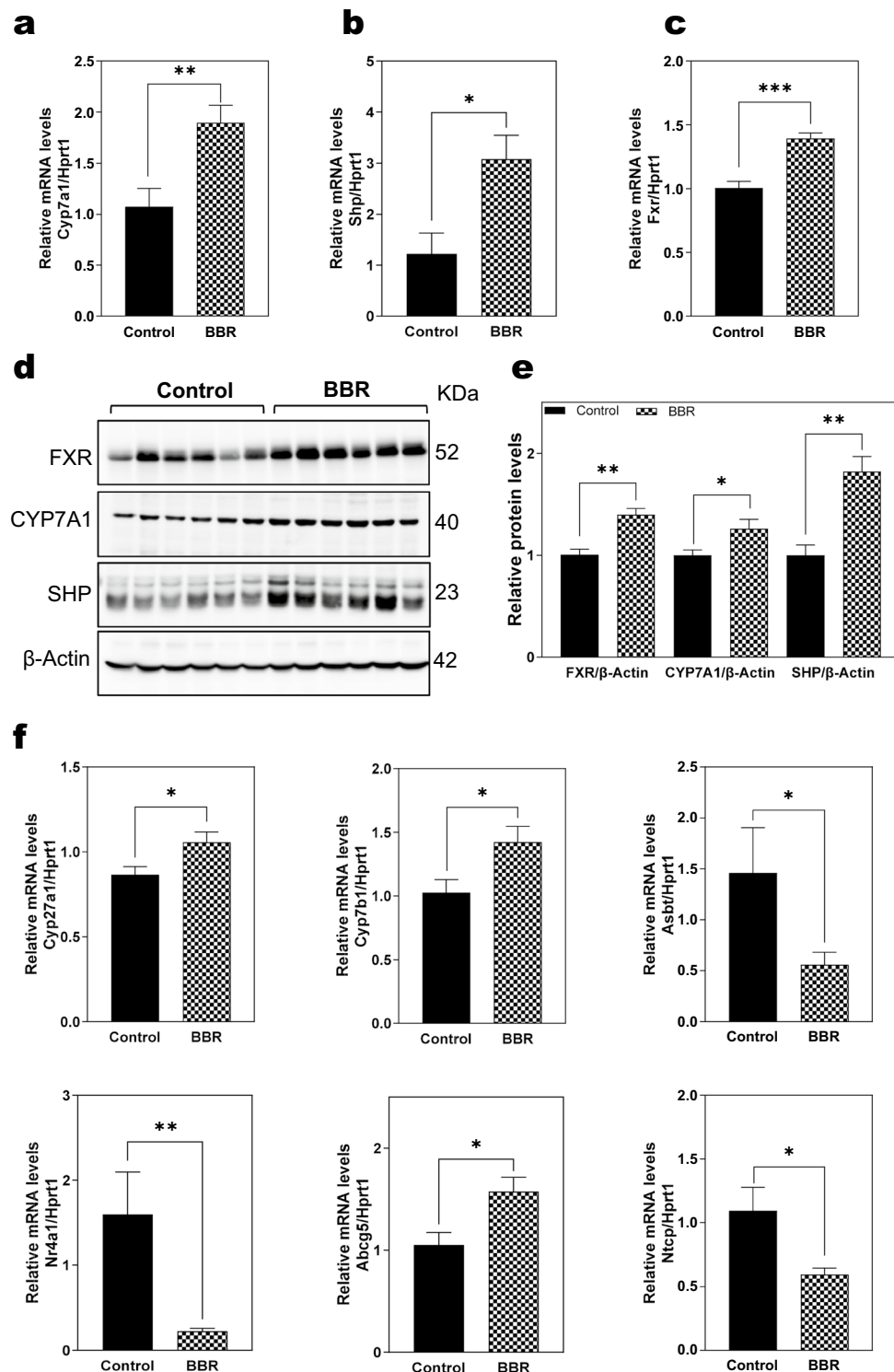
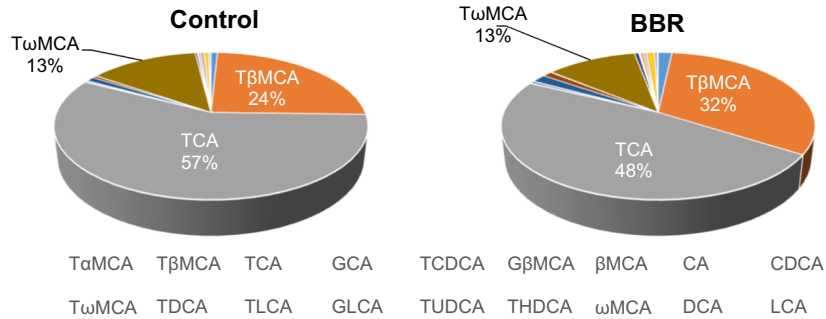
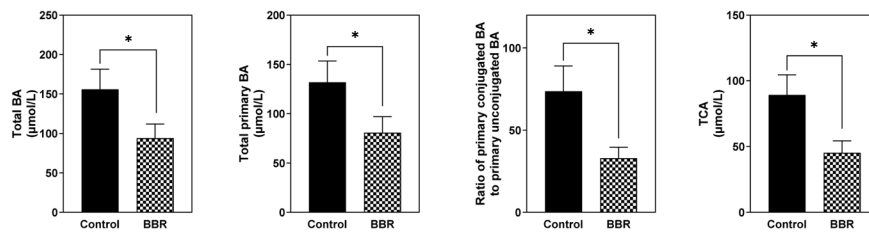


Fig. 6 Effect of BBR on bile acid metabolism in *Mdr2*^{-/-} mice. **a–c**, **f** Relative mRNA levels of key genes involved in bile acid metabolism in the liver, including *Cyp7a1*, *Shp* (*Nr0b2*), *Fxr* (*Nr1h4*), *Cyp27a1*, *Cyp7b1*, *Asbt*, *Nr4a1*, *Abcg5*, and *Ntcp*. The mRNA levels were determined by qRT-PCR and normalized with *HPRT1* as an internal control. **d** Representative immunoblot images of *FXR*, *SHP*, *CYP7A1* and β -Actin are shown. **e** The relative protein levels of *FXR*, *SHP*, and *CYP7A1* were calculated using β -actin as a loading control. Data are expressed as the mean \pm SEM. Statistical significance relative to Control: * $p < 0.05$, ** $p < 0.01$, *** $p < 0.001$ ($n = 9–12$)

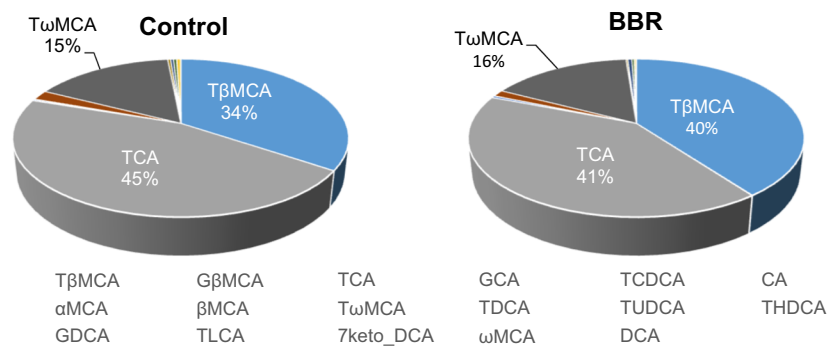
a Bile acid profile in the serum



b Bile acids in the serum



c Bile acid profile in the liver



d Bile acids in the liver

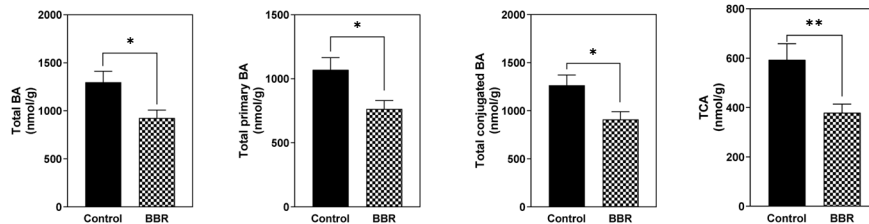


Fig. 7 Impact of BBR on bile acid homeostasis in *Mdr2^{-/-}* mice. Serum and liver tissues were processed for bile acids (BA) analysis using liquid chromatography-tandem mass spectrometry (LC-MS/MS). **a** BA composition profile in the serum, expressed as a percentage of total BA. **b** Total BA, total primary BA, the ratio of primary conjugated BA to primary unconjugated BA, and TCA in the serum. **c** BA composition profile in the liver, expressed as a percentage of total BA. **d** Total BA, total primary BA, total conjugated BA, and TCA in the liver. Data are expressed as the mean ± SEM. Statistical significance relative to control: **p* < 0.05, ***p* < 0.01 (n = 9–12)

intestine, and feces using LC–MS/MS. In the serum, as shown in Fig. 7a, BBR modulated the BAs composition by slightly reducing the percentage of taurocholic acid (TCA) in total BAs (from 57 to 48%) and increasing the percentage of tauro- β -muricholic acid (T β MCA) (from 24 to 32%). Among the individual BAs, the levels of TCA and tauro- ω -muricholic acid (T ω MCA) were significantly decreased by BBR (Additional file 2: Table S2, Fig. 7b). The results further showed that BBR was able to decrease the total BAs, total primary BAs, the ratios of primary conjugated BAs to primary unconjugated BAs, etc. (Additional file 2: Table S3). In the liver, BBR slightly modulated the BAs composition by regulating the composition of TCA and T β MCA (Fig. 7c). As shown in Additional file 2: Table S4, Fig. 7d, the levels of TCA were significantly reduced by BBR. In addition, BBR was able to decrease the total BAs, total primary BAs, total conjugated BAs, etc. (Additional file 2: Table S5, Fig. 7d). In the intestine, as shown in Additional file 1: Fig. S12a, BBR modified the BA composition by slightly reducing the percentage of TCA in total BAs (from 37 to 30%). The total BAs, total primary BAs, total conjugated BAs, and TCA were also reduced by BBR (Additional file 1: Tables S6, S7 and Fig. S12b). In the feces, as shown in Additional file 1: Fig. S12c, the BA composition remained unchanged after BBR treatment. However, BBR was able to increase the total BAs, total secondary BAs, TCA, etc. (Additional file 2: Tables S8, S9 and Additional file 1: Fig. S11d). Interestingly, lithocholic acid (LCA), which has high cytotoxicity [28], was significantly increased in fecal samples of BBR. However, LCA is hydrophobic and mostly remains in the fecal pellet.

BBR enhances intestinal barrier function and reduces bacterial translocation in *Mdr2*^{-/-} mice

Compromised intestinal barrier integrity leads to bacterial migration to the liver, other organs and the bloodstream, causing systemic inflammation [7]. As shown in Fig. 8A, BBR treatment significantly reduced gut permeability in *Mdr2*^{-/-} mice, indicated by lower serum levels of fluorescein isothiocyanate (FITC)-Dextran. Additionally, bacteria presence in the mesenteric lymph nodes (MLNs) and blood was investigated. Notably, BBR treatment markedly decreased bacterial translocation to the MLNs (Fig. 8b). This reduction was consistent with fewer bacteria observed in the blood of BBR-treated *Mdr2*^{-/-} mice compared to untreated *Mdr2*^{-/-} mice (Fig. 8c). H&E staining revealed that *Mdr2*^{-/-} mice treated with BBR exhibited less lymphatic vessel dilation and inflammatory cell infiltration in their small intestines compared to untreated *Mdr2*^{-/-} mice (Fig. 8d). Additionally, BBR treatment was associated with increased mucus layer thickness, as evidenced by enhanced mucin-2 expression

identified through Alcian blue staining (Fig. 8e). Immunofluorescence staining of the tight junction protein ZO-1 showed that BBR restored the integrity of tight junctions in the small intestines of these mice (Fig. 8f). Gene expression analysis further confirmed BBR's anti-inflammatory effects, with reduced mRNA levels of several inflammation-related genes (*Mcp-1*, *Cd11b*, *Il-1 β* , *Vcam-1*, *Il-1 α* , *Cxcl1*) in the small intestine of BBR-treated mice (Additional file 1: Fig. S13a). Notably, the expression levels of *Asbt*, *Chop*, and the lncRNA *H19* were also decreased in these mice following BBR treatment (Additional file 1: Fig. S13b).

BBR accumulates in the intestinal tract and modifies gut microbiome in *Mdr2*^{-/-} mice

In light of BBR's beneficial effects on the liver and intestine in *Mdr2*^{-/-} mice, we investigated its tissue distribution across various organs. After administering a single 50 mg/kg dose of BBR to these mice, we collected blood and major tissues at different time points for analysis (Additional file 2: Table S10). As shown in Additional file 1: Fig. S14a, the concentration of BBR in the serum was decreased gradually over time in *Mdr2*^{-/-} mice. Notably, BBR concentration was ~100-fold higher in the colon, intestine, and stomach, compared in the liver, kidney, heart, lung, brain, and spleen (Additional file 1: Fig. S14b). This suggests that BBR mitigates cholestatic liver injury by modulating the gut-liver axis, an important pathway influenced by the gut microbiome, which is crucial for BA deconjugation and excretion. Considering the role of the gut microbiome in PSC [1, 2, 6], we performed 16S rRNA gene sequencing. The analysis revealed that while Alpha diversity (gut microbiota structure within a community) showed no significant changes with BBR treatment (Additional file 1: Fig. S15a), Beta diversity (the comparison of gut microbiota structure between communities) displayed significant changes, though without a dose-dependent effect (Additional file 1: Fig. S15b and Table S11). The microbial composition in BBR-treated *Mdr2*^{-/-} mice showed a slight increase in *Bacteroidetes* (69% vs. 65% in the control group) and a decrease in *Firmicutes* (30% vs. 34% in the control group), indicating that BBR could modify the microbial structure (Additional file 1: Fig. S16).

Discussion

Cholestatic liver diseases, marked by reduced bile flow, manifest through inflammation, ductular proliferation, and fibrosis. Patients with PSC and concurrent inflammatory bowel diseases (IBDs) face a significantly higher risk of developing cholangiocarcinoma and colorectal cancer [1, 4]. Currently, there is no effective medication for improving transplant-free survival in these cases.

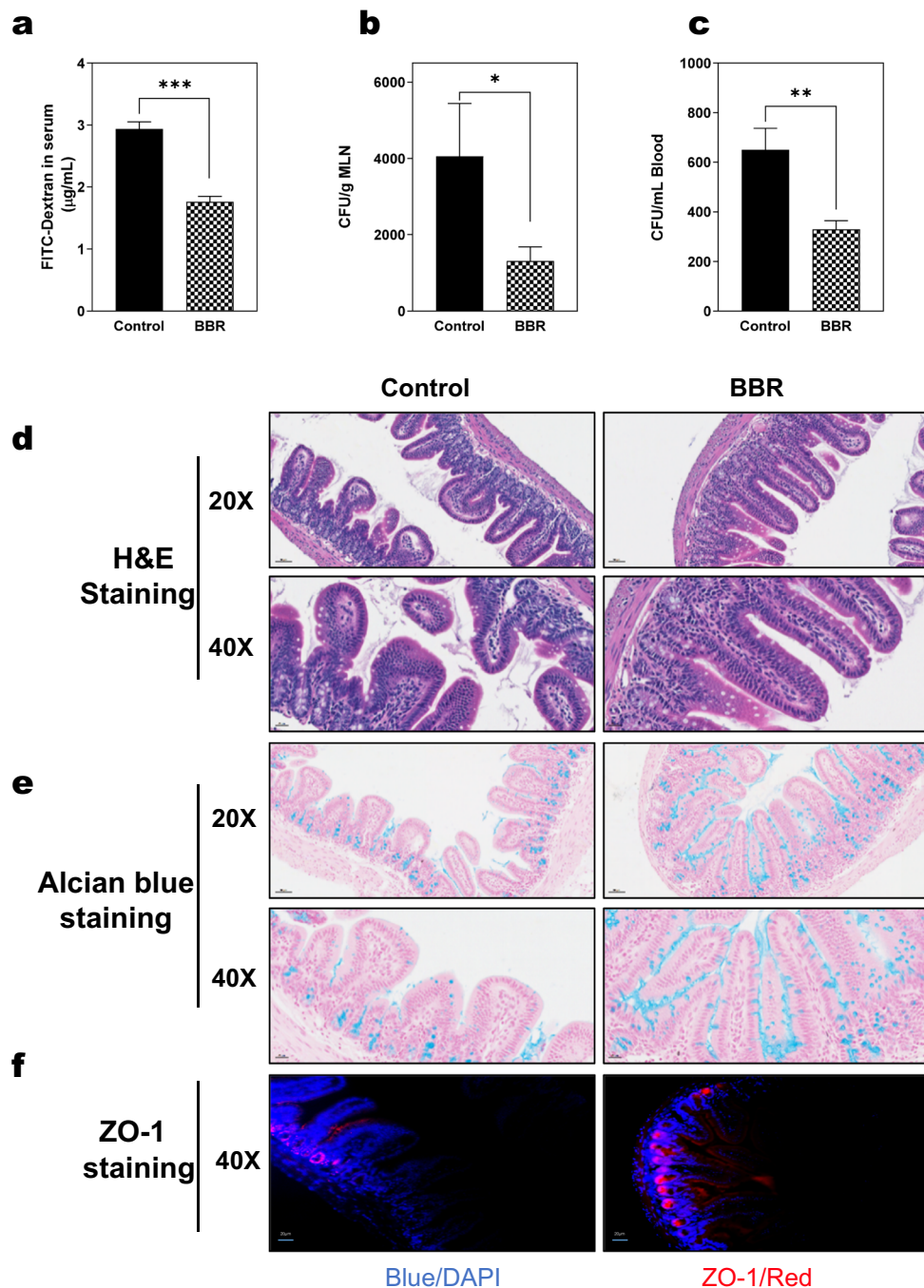


Fig. 8 Impact of BBR on intestinal barrier function and bacterial translocation in $Mdr2^{-/-}$ mice. **a** Serum levels of FITC-Dextran levels, a marker of intestinal permeability. **b-c** Colony-forming units (CFUs) of bacteria isolated from MLNs (mesenteric lymph node) and blood, respectively. **d** Representative images of H&E staining of small intestine sections (scale bar, 50 μ m for 20 \times and 20 μ m for 40 \times magnification). **e** Representative images of Alcian blue staining of small intestine sections (scale bar, 50 μ m for 20 \times and 20 μ m for 40 \times magnification). **f** Representative images of ZO-1 immunofluorescence (IF) staining of small intestine sections (scale bar, 20 μ m for 40 \times magnification). Data are expressed as the mean \pm SEM. Statistical significance relative to Control: * $p < 0.05$, ** $p < 0.01$, *** $p < 0.001$ ($n = 9-12$)

Liver transplantation is the only definitive treatment for PSC, though it carries a high risk of disease recurrence [2, 29, 30]. Recent studies suggest that targeting pathways,

such as BA synthesis and transport, hepatic inflammation, mitochondrial respiration, oxidative stress, intestinal inflammation, and gut microbiota, could provide new

therapeutic strategies for cholestatic liver diseases [26, 27, 31–35].

BBR has long been used in Asia as an anti-bacterial medicine. Clinical and preclinical studies highlight its potential in treating metabolic diseases by modulating various molecular targets, including transcription factors, cell survival/proliferative proteins, enzymes, metastatic/invasion molecules, growth factors, platelet activation, inflammatory cytokines, apoptotic proteins, protein kinases, receptors, and the others [14, 36]. There are a considerable number of studies demonstrating that BBR has preventive or therapeutic effects on various liver diseases, such as hepatitis, MAFLD, and liver fibrosis [11, 37–42]. However, its impact on cholestatic liver injury remains unexplored. To elucidate the therapeutic effect and potential mechanisms of BBR on cholestatic liver injury, we conducted a series of analyses, including histological imaging, biochemical analysis, molecular biology, and RNA-seq transcriptome analysis. Using bioinformatic tools, we identified differentially expressed genes regulated by BBR followed by GO, KEGG pathway, and functional category analysis. The findings of this study strongly suggest that BBR is potentially effective in treating cholestatic liver injury. The major mechanisms underlying BBR's beneficial effects include reducing bile duct injury and hepatic fibrosis, alleviating hepatic inflammation and ER stress, restoring BA homeostasis, and improving intestinal barrier function as well as modulating gut microbiome.

PSC is an inflammatory liver disease often associated with severe cholestatic liver injury [43]. BBR is known for its potent anti-inflammatory activities in liver disease [16, 17]. Key pathways, such as NF- κ B signaling pathway, MAPK pathways, and oxidative phosphorylation, are involved in inflammation-driven cholestatic liver injury [8, 23, 44, 45]. Our RNA-seq gene analysis and pathway profiling showed that BBR significantly reduced inflammation in *Mdr2*^{-/-} mice. This reduction is achieved through BBR's ability to inhibit inflammatory macrophage infiltration in the liver, which is evident from the decreased expression of various chemokines, cytokines, and cell surface adhesion molecules (Fig. 4, Additional file 1: Fig. S6). Additionally, BBR modulates NF- κ B signaling, the MAPK signaling pathway, and oxidative phosphorylation (Additional file 1: Fig. S7–S9).

CCL2/MCP-1 chemokines, produced by fibroblasts, activated cholangiocytes, resident macrophages, and endothelial cells, play a crucial role in the inflammatory response. A recent study suggests that targeting the CCR2/CCL2 axis can limit monocyte recruitment and reduce fibrosis and cholestasis, offering a potential treatment approach for PSC [46]. In line with these findings, our study demonstrates that BBR suppresses the hepatic

expression of CCR2 and CCL2. Furthermore, the ER stress response, a key factor in inflammation and metabolic disorders, is significantly modulated by BBR [24, 47, 48]. Disruptions in ER homeostasis activate the UPR, leading to inflammation and cell injury. The IRE1, protein kinase RNA-like ER kinase (PERK), and ATF6 pathways are the three major branches of the UPR [24]. BBR has been previously shown to inhibit HIV protease inhibitor-induced ER stress in macrophages and inhibit free fatty acid and LPS-induced inflammation via modulating the PERK-ATF4-CHOP signaling pathway in macrophages and hepatocytes [17, 18]. Consistently, our current study found that BBR significantly reduced ER stress in *Mdr2*^{-/-} mice, particularly inhibiting the PERK-ATF4-CHOP pathway (Fig. 5 and Additional file 1: Fig. S10).

BA homeostasis is crucial in managing cholestatic liver diseases [3, 49]. BAs are synthesized in hepatocytes and immediately secreted into bile through the bile duct. The majority of BAs are reabsorbed in the terminal ileum and transported back to the liver through portal vein. The enterohepatic circulation of BA is an important physiological process, making the synthesis and transport of BAs vital targets for cholestatic liver injury [50, 51]. Our studies show that BBR can restore BA homeostasis by modulating key enzymes, nuclear receptors, and hepatic transporters involved in BA synthesis and transport (Fig. 6 and Additional file 1: Fig. S11). Elevated serum BA levels, particularly total, primary, conjugated BAs, including TCA, were common in PSC patients [52–54]. The current study showed that BBR treatment in *Mdr2*^{-/-} mice significantly reduced these BA levels in serum, liver, and small intestine while increasing fecal BA output without causing diarrhea (Fig. 7 and Additional file 1: Fig. S12). This suggests BBR's role as a differential BA transport inhibitor, indicated by reduced *Ntcp* and *Asbt* expression (Fig. 6). Furthermore, BBR has been shown to influence key regulators of BA homeostasis significantly. In our study, BBR increased the expression of *Fxr α* , a crucial regulator in BA homeostasis, and increased the expression of *Shp*, which represses *Cyp7a1* by inhibiting LRH-1 activity [55, 56]. However, the RNA-seq data showed BBR had no significant effects on LRH-1, but upregulated both *Cyp7a1* and *Cyp27a1* levels in the liver (Fig. 6). These results suggest the potential compensatory mechanisms to counteract the inhibition of BA up taking in *Mdr2*^{-/-} mice with BBR treatment. Although FXR agonists and ASBT inhibitors have been tested in clinical trials for various liver diseases, the potential to treat PSC remains uncertain. Our previous studies reported that increased primary conjugated BA is responsible for cholestatic liver injury and liver fibrosis via activating sphingosine-1 phosphate receptor 2 (*S1PR2*), which can

upregulate lncRNA H19 in *Mdr2*^{-/-} mice [57–60]. Our recent study showed that BBR reduced the expression of H19 in a MASH mouse model [16]. Consistently, in this study, our results showed that H19 was inhibited by BBR treatment in *Mdr2*^{-/-} mice.

Recent clinical studies have established a link between disrupted intestinal barrier function, bacterial translocation, and the progression of cholestatic liver diseases, such as PSC and PBS [61]. Specifically, in *Mdr2*^{-/-} mice, impairment in intestinal barrier function has been observed, including diminished tight junction protein expression, reduced mucus layers, increased permeability, and enhanced bacterial translocation [9]. Our previous study has reported that ER stress-induced activation of CHOP leads to disruption of intestinal barrier function, bacterial translocation, activation of inflammation, and eventually results in fibrosis in the liver [7]. In line with these findings, our current study demonstrates that BBR effectively decreased CHOP expression in both the liver and intestine (Fig. 5d and Additional file 1: Fig. S13b), suggesting its potential to mitigate these pathological processes. Moreover, recent studies reported that H19 exacerbates intestinal barrier dysfunction by inhibiting autophagy and impairing goblet and Paneth cell functions [62, 63]. Consistent with this, our results show that BBR significantly inhibits H19, correlating with restored epithelial barrier function as evidenced by increased expression of mucin-2 and ZO-1 (Figs. 8e-f & Additional file 1: Fig. S13b).

A previous study using hamsters found that orally administered BBR predominantly accumulates in the gut rather than in circulation, significantly affecting both gut and circulatory metabolites despite low serum levels [64]. Our study aligns with these findings, showing that BBR concentrations are highest in the stomach, intestine, and colon and relatively lower in the liver, kidney, heart, lung, brain, and spleen. This suggests that BBR mitigates cholestatic liver injury by modulating the gut-liver axis (Additional file 1: Fig. S14). It is well established that the gut microbiota regulates BA composition and levels, particularly in PSC. BBR has been reported to have antidiabetic effects by modulating the gut microbiome [10, 15]. Our current study further indicates that BBR alters the gut microbiota composition in *Mdr2*^{-/-} mice. Specifically, BBR increased the relative abundance of *Bacteroidetes* and decreased that of *Firmicutes* (Additional file 1: Fig. S15), which is significant as bacteria in *Firmicutes* are known for high bile salt hydrolase (BSH) activity, promoting BA deconjugation and fecal excretion [65, 66]. This alteration in microbiota composition aligns with the interplay between intestinal microbiota and BAs, where each influence the other.

Conclusion

In summary, our study sheds light on the potential mechanisms by which BBR attenuates cholestatic liver injury in a PSC mouse model. As illustrated in Fig. 9, BBR can directly or indirectly target various liver cells, including hepatocytes, macrophages, stellate cells, and cholangiocytes, modulating multiple pathways related to bile duct injury, fibrosis, inflammation, ER stress, and BA metabolism and transport in the gut-liver-axis. Furthermore, BBR enhances intestinal barrier function and reduces bacterial translocation, while also restoring BA homeostasis and gut microbiota. These findings suggest that BBR has potential as a pharmacological treatment for cholestatic liver injury such as PSC.

Materials and methods

Reagents

Berber chloride hydrate (BBR) was purchased from Sigma (St. Louis, MO, USA, Cat #14050). Common laboratory chemicals were purchased from Sigma Aldrich (St. Louis, MO, USA). All antibodies used in this study are listed in Additional file 2: Table S1.

Animal experiments

FVB *Mdr2*^{-/-} mice (100 days old, both sexes, n=9–12) were originally obtained from Dr. Gianfranco Alpini (Texas A&M HSC College of Medicine). *Mdr2*^{-/-} mouse (C57/BL6 background) is a kind gift from Dr. Daniel Goldenberg at the Department of Pathology, Hadassah-Hebrew University Medical Center, Jerusalem, Israel. Mice were randomly divided into the vehicle control group and BBR group. Mice were treated with BBR (50 mg/kg) or vehicle (0.5% carboxyl methyl cellulose sodium solution) by intragastric administration once daily for 8 weeks. All mice were housed in a 12 h light/12 h dark cycle with a controlled room temperature between 21 and 23 °C and free access to water. All the experimental procedures were performed according to protocols approved by the Richmond VA Medical Center and Virginia Commonwealth University Institutional Animal Care and Use Committee. All animal experiments were performed in accordance with institutional guidelines for ethical animal studies. At the end of the experiment, mice were weighed and anesthetized by exposure to inhaled isoflurane. The blood was collected by cardiac puncture. The serum was collected and stored at -80 °C for later analysis. After euthanasia, the liver and small intestine were collected for histological analysis, RNA profiling, and Western blot analysis. Fecal samples were collected for 16S rRNA gene sequencing to measure the gut microbiome.

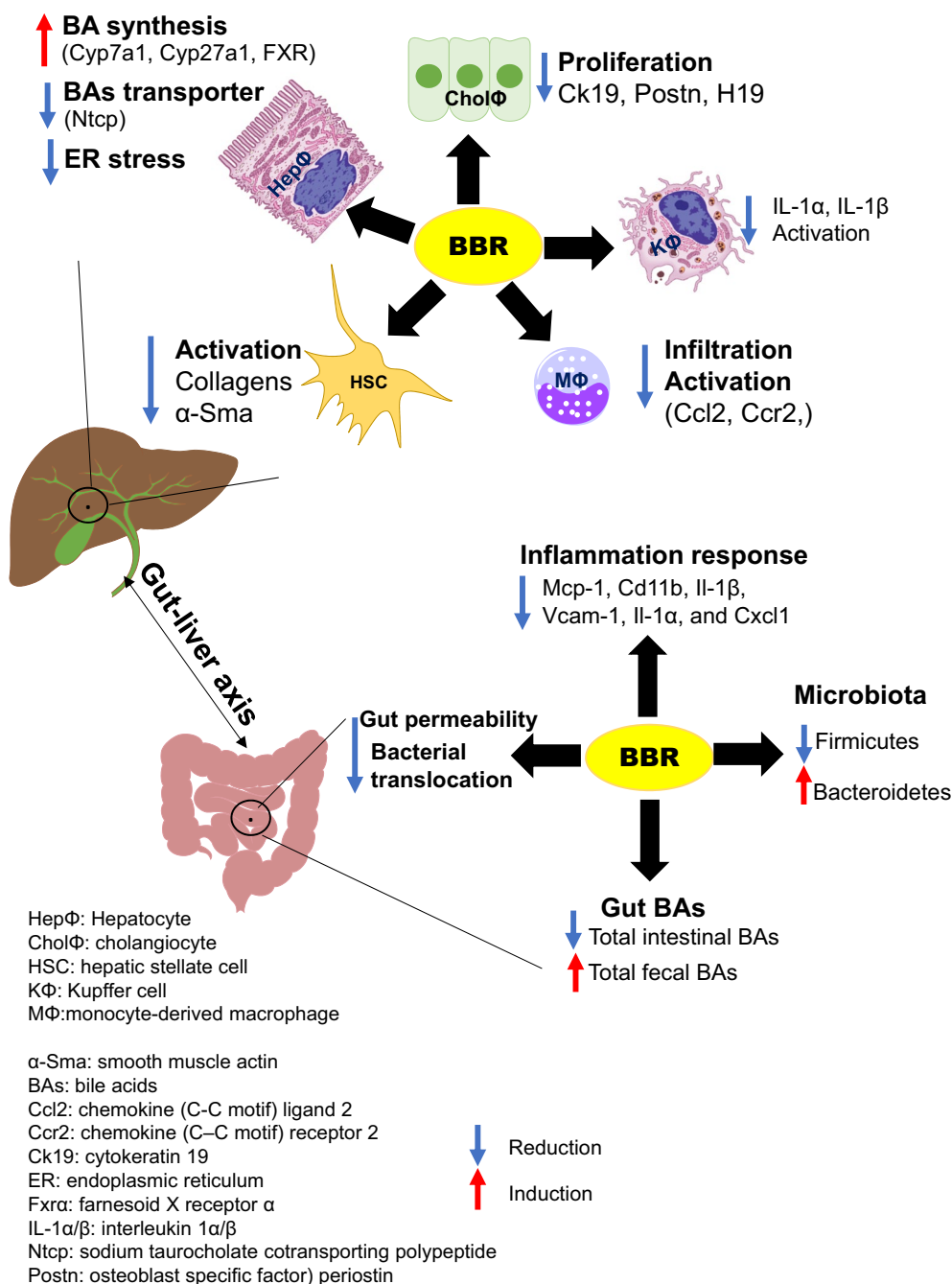


Fig. 9 Schematic Representation of BBR’s Potential Mechanisms in Alleviating Cholestatic Liver Injury. This diagram illustrates the proposed molecular and cellular mechanisms through which BBR mitigates cholestatic liver injury in a mouse model of sclerosing cholangitis. It visually summarizes the pathways and interactions influenced by BBR treatment, highlighting its multifaceted role in addressing liver disease pathology

RNA sequencing (RNAseq) and bioinformatic analysis

Total liver RNA was isolated using Chemagic Prepito®-D Nucleic Acid Extractor (PerkinElmer, Waltham, MA, USA) with a Prepito RNA kit (PerkinElmer, USA). The RNAseq with ribosomal RNA (rRNA) depletion was done by Genewiz Company using

the Illumina HiSeq® X platform (Genewiz Co., South Plainfield, NJ, USA). Sequencing reads were trimmed and filtered using bbdduk to remove adapters and low-quality reads. Reads from mouse samples were mapped to Ensembl GRCm38 transcripts annotation (release 82), using RSEM. Gene expression data normalization

and differential expression analysis were performed using the R package edgeR. Significantly up- or down-regulated genes were determined as fold change ≥ 2 and p -value < 0.05 . Hierarchical clustering was performed to show distinguishable mRNA expression profiles among the samples (Heatmap was plotted by <http://www.bioinformatics.com.cn>, an online platform for data analysis and visualization). The volcano graph and heatmaps were created to visualize significantly dys-regulated mRNAs using GraphPad Prism (version 8; GraphPad Software Inc., San Diego, CA, USA). Gene Ontology (GO) analysis was used to investigate three functionality domains: biological process (BP), cellular component (CC), and molecular function (MF) using DAVID (Database for Annotation, Visualization, and Integrated Discovery) v6.8 (<https://david.ncifcrf.gov/>). Pathway analysis was performed to functionally analyze and map genes to Kyoto Encyclopedia of Genes and Genomes (KEGG) pathways (<https://pathview.uncc.edu/>).

Serum biochemical analysis and hepatic hydroxyproline content measurement

The serum levels of ALP, AST and ALT, total triglyceride (TG), total cholesterol (TC), very-low-density lipoprotein (VLDL), and ALB were determined using the Alfa Wassermann Vet ACE Axcel[®] System with commercially available assay kits (Alfa Wassermann diagnostic technologies, NJ, USA). To quantify liver fibrosis, hepatic hydroxyproline was measured using the Hydroxyproline Assay kit (Sigma Aldrich, MO, USA) according to the manufacturer's instructions.

Histological and immunohistochemical staining

Liver tissues were processed for hematoxylin and eosin (H&E) staining and immunohistochemistry (IHC) staining for CK-19 and Ki67 at the Mouse Model Core at the VCU Massey Cancer Center (Richmond, VA, USA). Picro Sirius Red Staining was performed using the commercial Kit (Abcam, USA) with the paraffin-embedded tissue sections according to the manufacturer's instructions. Small intestine tissues were processed for H&E staining. Alcian blue staining was performed using the Alcian blue Stain Kit (Abcam, USA). Immunofluorescence staining of ZO-1 was performed with the paraffin-embedded tissue sections according to the manufacturer's instructions. All the stained slides were scanned using a Vectra Polaris Automated Quantitative Pathology Imaging System (Akoya Biosciences, MA, USA), and the images were captured using Phenochart software (Akoya Biosciences, MA, USA).

Bile acid (BA) analysis

The serum, liver tissues, intestine contents, and colon feces were processed for BA analysis, as described previously [16]. The composition and levels of BAs in serum, liver, intestine and fecal samples were measured using a Shimadzu liquid chromatography/tandem mass spectrometric (LC-MS/MS) 8600 system as described previously [16]. Data were collected and processed using Lab Solutions software.

Tissue distribution of BBR

Mdr2^{-/-} mice were treated with BBR (50 mg/kg) by intragastric administration after a 12-h fast. Blood, heart, lung, liver, kidney, brain, spleen, stomach, intestine, colon, and feces were collected after 3, 6, 9, and 12 h of BBR treatment, respectively. The contents of BBR in serum and tissues were analyzed using LC-MS/MS.

A reliable LC-MS/MS method was developed and validated to quantify BBR, using L-tetrahydropalmatine as the internal standard (IS). To quantify BBR in the serum, serum samples and IS were incubated with acetonitrile/methanol/water 1 (1/1, v/v) in a 1.5 mL vial. For quantification of BBR in the spleen, lung, kidney, heart, stomach contents, intestine contents, and feces, tissue samples were incubated with acetonitrile/methanol (1/1, v/v) in a 2 mL vial with beads. The homogenized samples and IS were mixed with acetonitrile/methanol/water (1/1, v/v) in a 1.5 mL vial. After centrifugation at 12,000×g for 2 min at room temperature, the supernatant was filtered through 0.2 μ m PTFE membrane, and 2 μ L aliquots were injected into the LC-MS/MS system. The analyte was separated on a C18 reverse phase column and analyzed in the multiple reaction monitoring (MRM) mode using ESI with positive ionization, m/z 335.9 \rightarrow 320.1 for BBR and m/z 355.9 \rightarrow 192.2 for IS. Mobile phase A was 0.05% acetic acid in water, while mobile phase B was acetonitrile. The gradient was optimized at 30% to 75% B in 2 min and then maintained 75% B for 0.5 min. The column was equilibrated with 30% B for 1.5 min. Data were collected and processed using Lab Solutions software.

Quantitative RT-PCR

Total liver RNA was isolated using Chemagic Prepito[®]-D Nucleic Acid Extractor (PerkinElmer, USA) with Prepito RNA kit (PerkinElmer, USA). cDNA synthesis and Quantitative RT-PCR analysis of relative mRNA expression levels of target genes were previously described [16]. Primer sequences will be provided upon request.

Immunoblotting analysis

Total proteins were prepared using cold RIPA buffer. Nuclear proteins were isolated, as previously described.

Protein concentration was measured using the Bio-Rad Protein Assay reagent. Proteins were resolved on 10% SDS-PAGE and transferred to nitrocellulose membranes (Thermo, Waltham, MA, USA). 5% milk was used to block the background. The target proteins were probed with the specific primary antibodies and detected using HRP-conjugated secondary antibodies and ECL reagents (Thermo, USA). Images were captured using the Bio-Rad Gel Doc XR+ Imaging System (Hercules, CA, USA). The density of immunoblotted bands was analyzed using Bio-Rad Image Lab computer software and normalized with histone 3 or β -Actin.

FITC-Dextran permeability and bacterial translocation assay

FITC-Dextran solution (100 mg/mL) was prepared in PBS. FITC-Dextran was administered to mice by oral gavage (600 mg/kg) and blood samples were taken after 4 h. The serum concentration of FITC-dextran was measured using Victor Multilabel Plate Counter (PerkinElmer, Waltham, MA) with an excitation wavelength of 490 nm and an emission wavelength of 530 nm. Blood and mesenteric lymph nodes (MLNs) were harvested in sterile conditions. Blood and homogenized MLNs were diluted in series and plated on Blood Agar Plates. After 72 h incubation at 37 °C in aerobic conditions, colony-forming units (CFUs) were counted and calculated.

Microbiota analysis

Fecal samples of $Mdr2^{-/-}$ mice treated with BBR 50 mg/kg or 100 mg/kg for 8 weeks were collected for 16S rRNA gene sequencing. Extraction, library preparation, sequencing, and analysis were performed at Rutgers Center for Microbiome Analysis Core, New Jersey Institute for Food, Nutrition and Health. All DNA samples were quantified using the Qubit 1×dsDNA HS assay kit (Thermo Fisher Scientific), which measured DNA concentration based on the fluorescence intensity of a fluorescent dye binding to double-stranded DNA. DNA integrity was assessed using agarose gel electrophoresis.

Statistical analysis

Data are expressed as the mean \pm SEM from at least three independent experiments. The student's t-test was used to analyze the difference between the two groups by GraphPad Prism (version 8; GraphPad Software Inc., San Diego, CA). A p -value < 0.05 was considered statistically significant.

Abbreviations

HSC	Hepatic stellate cells
lncRNA	Long non-coding RNA
PBC	Primary biliary cholangitis

PSC	Primary sclerosing cholangitis
S1PR2	Sphingosine-1 phosphate receptor 2
SHP	Short heterodimer partner
TCA	Taurocholate sodium
WT	Wild type

Supplementary Information

The online version contains supplementary material available at <https://doi.org/10.1186/s13578-024-01195-8>.

Additional file 1: Fig. S1. Impact of BBR on body weight and serum albumin levels in FVB $Mdr2^{-/-}$ mice and cholestatic liver injury in C57/BL6 $Mdr2^{-/-}$ mice. $Mdr2^{-/-}$ mice with FVB background (Control) and $Mdr2^{-/-}$ mice with C57BL/6 background (Control BL) were treated with vehicle or BBR (50 mg/kg) via oral gavage once daily for 8 weeks, respectively. a Body weight change during the BBR treatment period of 8 weeks in FVB $Mdr2^{-/-}$ mice. b Serum albumin levels in FVB $Mdr2^{-/-}$ mice. c Liver functional enzyme levels in C57/BL6 $Mdr2^{-/-}$ mice. d Representative images of hematoxylin and eosin (H&E) staining of the liver slides (scale bar, 50 μ m for 20 \times , 20 μ m for 40 \times magnification) in $Mdr2^{-/-}$ BL mice. Data are expressed as the mean \pm standard error of the mean (SEM). Statistical significance relative to Control BL: * p < 0.05 (n=9-12). **Fig. S2.** Comparative analysis of differentially expressed genes (DEGs) in experimental groups. a Hierarchical clustering heatmaps for DEGs in FVBWT, $Mdr2^{-/-}$ and $Mdr2^{-/-}$ mice treated with BBR. RNA-seq data were normalized using a Z-score for tag counts, with red and blue colors representing high and low gene expression, respectively. b Volcano plots for the $Mdr2^{-/-}$ vs. WT group comparison. Red dots represent upregulated genes, green dots represent downregulated genes, and black dots represent genes not differentially expressed. c Venn diagram illustrating the overlap of DEGs between the two comparisons: $Mdr2^{-/-}$ vs. WT and BBR-treated $Mdr2^{-/-}$ vs. $Mdr2^{-/-}$ Control. In $Mdr2^{-/-}$ vs. WT, there were a total of 1937 DEGs, including 1260 upregulated and 677 down-regulated genes. In BBR-treated $Mdr2^{-/-}$ vs. $Mdr2^{-/-}$ Control, there were a total of 587 DEGs, comprising 300 upregulated and 287 down-regulated genes. A total of 373 DEGs were common between the two comparisons. **Fig. S3.** Ingenuity pathway analysis (IPA) in experimental groups. The DEG data set with FC ≥ 2 and p -value < 0.05 was used for IPA analysis. The top 10 activated pathways in $Mdr2^{-/-}$ control mice compared to WT mice and the top 10 inhibited pathways in BBR-treated $Mdr2^{-/-}$ mice compared to $Mdr2^{-/-}$ control mice are shown. **Fig. S4.** Impact of BBR on hepatic fibrosis. a Representative images of liver sections stained with Picro-Sirius Red and CK19 IHC (scale bar, 100 μ m for 10 \times magnification) and processed images for quantification. b Hepatic hydroxyproline levels. Data are expressed as the mean \pm SEM. Statistical significance relative to control: * p < 0.05 (n=9-12). **Fig. S5.** Impact of BBR on genes associated with hepatic fibrosis in $Mdr2^{-/-}$ mice. a Representative heatmap of key genes involved in hepatic fibrosis in the liver, comparing the BBR-treated group with the control group. The RNA-seq data were normalized using a Z-score for tag counts, with red and blue colors denoting up- and down-regulated gene expression, respectively. b Relative mRNA expression levels of fibrosis-related genes (Pai1, Col12a1, Sox9, Egr1, Egr2, Egr3, Hbegf, Cyr61, and P4ha1), normalized against HPRT1 as an internal control. Data are expressed as the mean \pm SEM. Statistical significance relative to control: * p < 0.05, ** p < 0.01, *** p < 0.001 (n=9-12). **Fig. S6.** Impact of BBR on genes associated with inflammation in $Mdr2^{-/-}$ mice. Representative heatmap depicting the expression of key genes involved in hepatic inflammation, comparing the liver tissues of $Mdr2^{-/-}$ mice treated with BBR to the control group. The RNA-seq data were normalized using a Z-score, with red indicating upregulated gene expression and blue indicating downregulated gene expression. **Fig. S7.** Impact of BBR on NF- κ B signaling pathway. KEGG pathway analysis was performed on RNA-seq data to analyze functionally and map genes involved in the NF- κ B signaling pathway. a NF- κ B signaling pathway in $Mdr2^{-/-}$ vs. WT. b NF- κ B signaling pathway in $Mdr2^{-/-}$ treated with BBR vs. $Mdr2^{-/-}$ Control. Red and green colors indicate upregulated and downregulated gene expression, respectively. **Fig. S8.** Impact of BBR on MAPK signaling pathway. KEGG pathway analysis was performed on RNA-seq data to analyze functionally and map genes involved in the MAPK signaling pathway. a MAPK signaling pathway in $Mdr2^{-/-}$ vs. WT. b

MAPK signaling pathway in *Mdr2*^{-/-} treated with BBR vs. *Mdr2*^{-/-} Control. Red and green colors indicate upregulated and downregulated gene expression, respectively. **Fig. S9.** Impact of BBR on Oxidative phosphorylation pathway. KEGG pathway analysis was performed on RNA-seq data to analyze functionally and map genes involved in the Oxidative phosphorylation pathway. a Oxidative phosphorylation pathway in *Mdr2*^{-/-} vs. WT. b Oxidative phosphorylation pathway in *Mdr2*^{-/-} treated with BBR vs. *Mdr2*^{-/-} Control. Red and green colors indicate up- and down-regulated gene expression, respectively. **Fig. S10.** Impact of BBR on Protein processing in endoplasmic reticulum. RNA-seq data were performed to analyze functionally and map genes involved in the Protein processing in the endoplasmic reticulum pathway using KEGG. a Protein processing in endoplasmic reticulum pathway in *Mdr2*^{-/-} Control vs. WT. b Protein processing in endoplasmic reticulum pathway in *Mdr2*^{-/-} treated with BBR vs. *Mdr2*^{-/-} Control. Red and green colors indicate up- and down-regulated gene expression, respectively. **Fig. S11.** Impact of BBR on BA Metabolism. Representative heatmap of key genes involved in bile acid metabolism in the liver of BBR-treated vs. Control *Mdr2*^{-/-} mice. A Z-score is calculated for the RNA-seq data to normalize tag counts. Red and blue colors indicate up- and down-regulated gene expression, respectively. **Fig. S12.** Impact of BBR on bile acid homeostasis in *Mdr2*^{-/-} mice. The small intestine and feces were processed for BA analysis using LC-MS/MS. a BA composition profile in the small intestine is expressed as a percentage of total BA. b Total BA, total primary BA, total conjugated BA, and TCA in the small intestine. c BA composition profile in the feces is expressed as a percentage of total BA. d Total BA, total secondary BA, TCA, and LCA in the feces. Data are expressed as the mean ± SEM. Statistical significance relative to control: **p* < 0.05 (n=9-12). **Fig. S13.** Effect of BBR on inflammation and ER stress in the intestine of *Mdr2*^{-/-} mice. Relative mRNA levels of key genes involved in inflammation and ER stress in the intestine were determined by real-time RT-PCR and normalized with HPRT1 as an internal control. a The relative mRNA levels of *Mcp-1*, *Cd11b*, *Il-1β*, *Vcam-1*, *Il-1α*, and *Cxcl1*. b Relative mRNA levels of *Asbt*, *Chop* and *H19*. Data are expressed as the mean ± SEM. Statistical significance relative to Control: **p* < 0.05 (n=9-12). **Fig. S14.** Tissue distribution of BBR in *Mdr2*^{-/-} mice. *Mdr2*^{-/-} mice were treated with BBR (50 mg/kg, n = 3) by intragastric administration after a 12-h fast. Blood, spleen, brain, lung, heart, kidney, liver, stomach contents, intestine contents, and colon feces were collected at 3, 6, and 9 h post-treatment. The concentrations of BBR in the serum and various tissues were quantified using LC-MS/MS. a BBR concentration in the serum. b BBR concentration in the tissues. Data are expressed as the mean ± standard error of the mean (SEM). **Fig. S15.** Analysis of Fecal Microbiota Diversity in *Mdr2*^{-/-} Mice Treated with BBR. Fecal samples of FVB *Mdr2*^{-/-} mice treated with either 50 mg/kg or 100 mg/kg of BBR for 8 weeks were subjected to 16S rRNA gene sequencing to assess microbiota composition. a Alpha diversity of the fecal microbiota, presented through various metrics: Shannon Index (a), observed Amplicon Sequence Variants (ASVs) (b), Faith's phylogenetic diversity (c), and evenness (d). b Beta diversity analysis using Principal Coordinates Analysis (PCoA) plots, which illustrate variations in microbial communities. These plots are based on different distance metrics: Bray-Curtis distance (a), Jaccard distance (b), Weighted UniFrac distance (c), and Unweighted UniFrac distance (d), with each plot depicting variations along two principal coordinates that account for most of the variation. **Fig. S16.** Influence of BBR on the Proportions of Firmicutes and Bacteroidetes in the Gut Microbiota of *Mdr2*^{-/-} mice. The pie chart shows the relative percentages of the Firmicutes and Bacteroidetes phyla in the gut microbiota of *Mdr2*^{-/-} mice. Comparative analysis is shown across three groups: control, BBR-treated at 50 mg/kg, and BBR-treated at 100 mg/kg. This visualization highlights the specific shifts in these major bacterial phyla due to BBR treatment.

Additional file 2. Supplement tables with captions.

Acknowledgements

We thank Mrs. Elaine Kennedy for proofreading and English editing. We thank the Cancer Mouse Models Core of VCU Massey Cancer Center for histological service and technical support. We thank Dr. Daniel Goldenberg at the Department of Pathology, Hadassah-Hebrew University Medical Center, Jerusalem, Israel for providing C57/BL6 *Mdr2*^{-/-} mice. We thank Drs. Liping Zhao at Rutgers

Center for Microbiome Analysis Core, New Jersey Institute for Food, Nutrition and Health for microbiome analysis.

Author contributions

YW, WC, XZ and HZ conceived the original ideas, designed the study, analyzed the data, and wrote the manuscript; YW, DZ, LS, YT, GWW, JZ, QY, YX, XW, and ECG carried out the experiments and data analysis. JL, JL, GWW, YX helped with RNAseq data analysis and process; XZ and PBH reviewed the manuscript.

Funding

This study was supported by VA Merit Award I01BX004033 and 5I01BX005730; ShEEP grant (1 IS1 BX004777-01); National Institutes of Health Grant R01 DK104893, DK115377, 2R56DK115377-05A1, NIH-NCI Cancer Center Support Grant P30 CA 016059. Dr. Zhou is the recipient of a Research Career Scientist Award from the Department of Veterans Affairs (IK6BX004477).

Availability of data and materials

Detailed methods and datasets generated and/or analyzed during the current study are available in Additional file.

Declarations

Ethics approval and consent to participate

All animal experiments were performed following institutional guidelines for ethical animal studies and approved by the Virginia Commonwealth University Institutional Animal Care and Use Committee, Virginia, USA.

Consent for publication

All authors reviewed and approved the final manuscript. All authors supported the publication of this manuscript.

Competing interests

The authors declare no competing financial interests.

Author details

¹Department of Microbiology and Immunology, Virginia Commonwealth University and Richmond Veterans Affairs Medical Center, 1220 East Broad Street, MMRB-5044, Richmond, VA 23298-0678, USA. ²School of Pharmaceutical Science, Anhui University of Chinese Medicine, Hefei, Anhui, China. ³Department of Endocrinology, Jiangsu Province Hospital of Chinese Medicine, Nanjing University of Chinese Medicine, Nanjing, China. ⁴Department of Biostatistics, Virginia Commonwealth University, Richmond, VA, USA. ⁵Department of Computer Science, University of Kentucky, Lexington, KY, USA.

Received: 28 November 2023 Accepted: 9 January 2024

Published online: 25 January 2024

References

- Karlsen TH, Folseraas T, Thorburn D, Vesterhus M. Primary sclerosing cholangitis—a comprehensive review. *J Hepatol.* 2017;67:1298–323.
- Dyson JK, Beuers U, Jones DEJ, Lohse AW, Hudson M. Primary sclerosing cholangitis. *The Lancet.* 2018;391:2547–59.
- Jansen PL, Ghallab A, Vartak N, Reif R, Schaap FG, Hampe J, Hengstler JG. The ascending pathophysiology of cholestatic liver disease. *Hepatology.* 2017;65:722–38.
- Wagner M, Fickert P. Drug therapies for chronic cholestatic liver diseases. *Annu Rev Pharmacol Toxicol.* 2020;60:503–27.
- Jungst C, Lammert F. Cholestatic liver disease. *Dig Dis.* 2013;31:152–4.
- Trauner M, Fuchs CD, Halilbasic E, Paumgartner G. New therapeutic concepts in bile acid transport and signaling for management of cholestasis. *Hepatology.* 2017;65:1393–404.
- Liu R, Li X, Huang Z, Zhao D, Ganesh BS, Lai G, Pandak WM, et al. C/EBP homologous protein-induced loss of intestinal epithelial stemness contributes to bile duct ligation-induced cholestatic liver injury in mice. *Hepatology.* 2018;67:1441–57.

8. Shearn CT, Orlicky DJ, Petersen DR. Dysregulation of antioxidant responses in patients diagnosed with concomitant Primary Sclerosing Cholangitis/Inflammatory Bowel Disease. *Exp Mol Pathol*. 2018;104:1–8.
9. Liao L, Schneider KM, Galvez EJ, Frissen M, Marschall H-U, Su H, Hatting M, et al. Intestinal dysbiosis augments liver disease progression via NLRP3 in a murine model of primary sclerosing cholangitis. *Gut*. 2019;68:1477–92.
10. Zhang Y, Gu Y, Ren H, Wang S, Zhong H, Zhao X, Ma J, et al. Gut microbiome-related effects of berberine and probiotics on type 2 diabetes (the PREMOTe study). *Nat Commun*. 2020;11:5015.
11. Xu X, Zhu XP, Bai JY, Xia P, Li Y, Lu Y, Li XY, Gao X. Berberine alleviates nonalcoholic fatty liver induced by a high-fat diet in mice by activating SIRT3. *FASEB J*. 2019;33:7289–300.
12. Sun R, Yang N, Kong B, Cao B, Feng D, Yu X, Ge C, et al. Orally administered berberine modulates hepatic lipid metabolism by altering microbial bile acid metabolism and the intestinal fxr signaling pathway. *Mol Pharmacol*. 2017;91:110–22.
13. Kong Y, Li L, Zhao LG, Yu P, Li DD. A patent review of berberine and its derivatives with various pharmacological activities (2016–2020). *Expert Opin Ther Pat* 2021.
14. Xu X, Yi H, Wu J, Kuang T, Zhang J, Li Q, Du H, et al. Therapeutic effect of berberine on metabolic diseases: Both pharmacological data and clinical evidence. *Biomed Pharmacother*. 2021;133: 110984.
15. Wolf PG, Devendran S, Doden HL, Ly LK, Moore T, Takei H, Nittono H, et al. Berberine alters gut microbial function through modulation of bile acids. *BMC Microbiol*. 2021;21:1–15.
16. Wang Y, Tai YL, Zhao D, Zhang Y, Yan J, Kakiyama G, Wang X, et al. Berberine prevents disease progression of nonalcoholic steatohepatitis through modulating multiple pathways. *Cells*. 2021;10:1.
17. Wang Y, Zhou X, Zhao D, Wang X, Gurley EC, Liu R, Li X, et al. Berberine inhibits free fatty acid and LPS-induced inflammation via modulating ER stress response in macrophages and hepatocytes. *PLoS ONE*. 2020;15: e0232630.
18. Zha W, Liang G, Xiao J, Studer EJ, Hylemon PB, Pandak WM Jr, Wang G, et al. Berberine inhibits HIV protease inhibitor-induced inflammatory response by modulating ER stress signaling pathways in murine macrophages. *PLoS ONE*. 2010;5: e9069.
19. Mauad TH, Van Nieuwkerk CM, Dingemans KP, Smit JJ, Schinkel AH, Notenboom RG, van den Bergh Weerman MA, et al. Mice with homozygous disruption of the mdr2 P-glycoprotein gene a novel animal model for studies of nonsuppurative inflammatory cholangitis and hepatocarcinogenesis. *Am J Pathol*. 1994;145:1237.
20. Popov Y, Patsenker E, Fickert P, Trauner M, Schuppan D. Mdr2 (Abcb4)^{-/-} mice spontaneously develop severe biliary fibrosis via massive dysregulation of pro- and antifibrogenic genes. *J Hepatol*. 2005;43:1045–54.
21. Smit J, Schinkel AH, Elferink RO, Groen A, Wagenaar E, Van Deemter L, Mol C, et al. Homozygous disruption of the murine mdr2 P-glycoprotein gene leads to a complete absence of phospholipid from bile and to liver disease. *Cell*. 1993;75:451–62.
22. Eaton JE, Talwalkar JA, Lazaridis KN, Gores GJ, Lindor KD. Pathogenesis of primary sclerosing cholangitis and advances in diagnosis and management. *Gastroenterology*. 2013;145:521–36.
23. Plkarsky E. NF-KB functions as a tumour promoter in inflammation-associated cancer. *Nature (Lond)*. 2004;431:461–6.
24. Zhou H, Liu R. ER stress and hepatic lipid metabolism. *Front Genet*. 2014;5:112.
25. Tamaki N, Hatano E, Taura K, Tada M, Kodama Y, Nitta T, Iwasako K, et al. CHOP deficiency attenuates cholestasis-induced liver fibrosis by reduction of hepatocyte injury. *Am J Physiol Gastrointest Liver Physiol*. 2008;294:G498–505.
26. Fuchs CD, Paumgartner G, Mlitz V, Kunczer V, Halilbasic E, Leditznig N, Wahlström A, et al. Colesevelam attenuates cholestatic liver and bile duct injury in Mdr2^{-/-} mice by modulating composition, signalling and excretion of faecal bile acids. *Gut*. 2018;67:1683–91.
27. Baghdasaryan A, Fuchs CD, Osterreicher CH, Lemberger UJ, Halilbasic E, Pahlman I, Graffner H, et al. Inhibition of intestinal bile acid absorption improves cholestatic liver and bile duct injury in a mouse model of sclerosing cholangitis. *J Hepatol*. 2016;64:674–81.
28. Yang R, Zhao Q, Hu DD, Xiao XR, Huang JF, Li F. Metabolomic analysis of cholestatic liver damage in mice. *Food Chem Toxicol*. 2018;120:253–60.
29. Mendes FD, Kim WR, Pedersen R, Therneau T, Lindor KD. Mortality attributable to cholestatic liver disease in the United States. *Hepatology*. 2008;47:1241–7.
30. Song J, Li Y, Bowlus CL, Yang G, Leung PSC, Gershwin ME. Cholangiocarcinoma in patients with primary sclerosing cholangitis (PSC): a comprehensive review. *Clin Rev Allergy Immunol*. 2020;58:134–49.
31. Li J, Zhu X, Zhang M, Zhang Y, Ye S, Leng Y, Yang T, et al. Limb expression 1-like (LX1L) protein promotes cholestatic liver injury by regulating bile acid metabolism. *J Hepatol*. 2021;75(2):400–13.
32. Tardelli M, Bruschi FV, Fuchs CD, Claudel T, Auer N, Kunczer V, Baumgartner M, et al. Monoacylglycerol lipase inhibition protects from liver injury in mouse models of sclerosing cholangitis. *Hepatology*. 2020;71:1750–65.
33. Liu Y, Chen K, Li F, Gu Z, Liu Q, He L, Shao T, et al. Probiotic Lactobacillus rhamnosus GG prevents liver fibrosis through inhibiting hepatic bile acid synthesis and enhancing bile acid excretion in mice. *Hepatology*. 2020;71:2050–66.
34. Pradhan-Sundt T, Kosar K, Saggi H, Zhang R, Vats R, Cornuet P, Green S, et al. Wnt/beta-catenin signaling plays a protective role in the Mdr2 knockout murine model of cholestatic liver disease. *Hepatology*. 2020;71:1732–49.
35. Miethke AG, Zhang W, Simmons J, Taylor AE, Shi T, Shanmukhappa SK, Karns R, et al. Pharmacological inhibition of apical sodium-dependent bile acid transporter changes bile composition and blocks progression of sclerosing cholangitis in multidrug resistance 2 knockout mice. *Hepatology*. 2016;63:512–23.
36. Feng X, Sureda A, Jafari S, Memariani Z, Tewari D, Annunziata G, Barrea L, et al. Berberine in cardiovascular and metabolic diseases: from mechanisms to therapeutics. *Theranostics*. 2019;9:1923–51.
37. Eissa LA, Kenawy HI, El-Karef A, Elsherbiny NM, El-Mihi KA. Antioxidant and anti-inflammatory activities of berberine attenuate hepatic fibrosis induced by thioacetamide injection in rats. *Chem Biol Interact*. 2018;294:91–100.
38. Hung TC, Jassey A, Liu CH, Lin CJ, Lin CC, Wong SH, Wang JY, et al. Berberine inhibits hepatitis C virus entry by targeting the viral E2 glycoprotein. *Phytomedicine*. 2019;53:62–9.
39. Zhu X, Bian H, Wang L, Sun X, Xu X, Yan H, Xia M, et al. Berberine attenuates nonalcoholic hepatic steatosis through the AMPK-SREBP-1c-SCD1 pathway. *Free Radic Biol Med*. 2019;141:192–204.
40. Chang X, Wang Z, Zhang J, Yan H, Bian H, Xia M, Lin H, et al. Lipid profiling of the therapeutic effects of berberine in patients with nonalcoholic fatty liver disease. *J Transl Med*. 2016;14:266.
41. Wu L, Xia M, Duan Y, Zhang L, Jiang H, Hu X, Yan H, et al. Berberine promotes the recruitment and activation of brown adipose tissue in mice and humans. *Cell Death Dis*. 2019;10:468.
42. Mai W, Xu Y, Xu J, Zhao D, Ye L, Yu G, Wang Z, et al. Berberine inhibits nod-like receptor family pyrin domain containing 3 inflammasome activation and pyroptosis in nonalcoholic steatohepatitis via the ROS/TXNIP Axis. *Front Pharmacol*. 2020;11:185.
43. Gulamhusein AF, Hirschfield GM. Primary biliary cholangitis: pathogenesis and therapeutic opportunities. *Nat Rev Gastroenterol Hepatol*. 2020;17:93–110.
44. Nemeth J, Stein I, Haag D, Riehl A, Longerich T, Horwitz E, Breuhahn K, et al. S100A8 and S100A9 are novel nuclear factor kappa B target genes during malignant progression of murine and human liver carcinogenesis. *Hepatology*. 2009;50:1251–62.
45. Li S, Wang R, Wu B, Wang Y, Song F, Gu Y, Yuan Y. Salvianolic acid B protects against ANIT-induced cholestatic liver injury through regulating bile acid transporters and enzymes, and NF-kappaB/IkappaB and MAPK pathways. *Naunyn Schmiedebergs Arch Pharmacol*. 2019;392:1169–80.
46. Guicciardi ME, Trusconi CE, Krishnan A, Bronk SF, Lorenzo Pisarello MJ, O'Hara SP, Splinter PL, et al. Macrophages contribute to the pathogenesis of sclerosing cholangitis in mice. *J Hepatol*. 2018;69:676–86.
47. Kim I, Xu W, Reed JC. Cell death and endoplasmic reticulum stress: disease relevance and therapeutic opportunities. *Nat Rev Drug Discov*. 2008;7:1013–30.
48. Dara L, Ji C, Kaplowitz N. The contribution of endoplasmic reticulum stress to liver diseases. *Hepatology*. 2011;53:1752–63.
49. Fickert P, Wagner M. Biliary bile acids in hepatobiliary injury - What is the link? *J Hepatol*. 2017;67:619–31.

50. Wang Y, Gunewardena S, Li F, Matye DJ, Chen C, Chao X, Jung T, et al. An FGF15/19-TFEB regulatory loop controls hepatic cholesterol and bile acid homeostasis. *Nat Commun.* 2020;11:3612.
51. Chiang JY. Bile acid metabolism and signaling. *Compr Physiol.* 2013;3:1191–212.
52. Ghonem NS, Auclair AM, Hemme CL, Gallucci GM, de la Rosa RR, Boyer JL, Assis DN. Fenofibrate improves liver function and reduces the toxicity of the bile acid pool in patients with primary biliary cholangitis and primary sclerosing cholangitis who are partial responders to ursodiol. *Clin Pharmacol Ther.* 2020;108:1213–23.
53. Mousa OY, Juran BD, McCauley BM, Vesterhus MN, Folseraas T, Turgeon CT, Ali AH, et al. Bile acid profiles in primary sclerosing cholangitis and their ability to predict hepatic decompensation. *Hepatology.* 2020;74(1):281–95.
54. Sanyal AJ, Ling L, Beuers U, DePaoli AM, Lieu HD, Harrison SA, Hirschfeld GM. Potent suppression of hydrophobic bile acids by aldafermin, an FGF19 analogue, across metabolic and cholestatic liver diseases. *JHEP Rep.* 2021;3: 100255.
55. Kuipers F, Claudel T, Sturm E, Staels B. The Farnesoid X Receptor (FXR) as modulator of bile acid metabolism. *Rev Endocr Metab Disord.* 2004;5:319–26.
56. Goodwin B, Jones SA, Price RR, Watson MA, McKee DD, Moore LB, Galardi C, et al. A regulatory cascade of the nuclear receptors FXR, SHP-1, and LRH-1 represses bile acid biosynthesis. *Mol Cell.* 2000;6:517–26.
57. Wang Y, Aoki H, Yang J, Peng K, Liu R, Li X, Qiang X, et al. The role of sphingosine 1-phosphate receptor 2 in bile-acid-induced cholangiocyte proliferation and cholestasis-induced liver injury in mice. *Hepatology.* 2017;65:2005–18.
58. Li X, Liu R, Huang Z, Gurley EC, Wang X, Wang J, He H, et al. Cholangiocyte-derived exosomal long noncoding RNA H19 promotes cholestatic liver injury in mouse and humans. *Hepatology.* 2018;68:599–615.
59. Li X, Liu R, Wang Y, Zhu W, Zhao D, Wang X, Yang H, et al. Cholangiocyte-derived exosomal lncRNA H19 promotes macrophage activation and hepatic inflammation under cholestatic conditions. *Cells.* 2020;9:1.
60. Liu R, Li X, Zhu W, Wang Y, Zhao D, Wang X, Gurley EC, et al. Cholangiocyte-derived exosomal long noncoding RNA H19 promotes hepatic stellate cell activation and cholestatic liver fibrosis. *Hepatology.* 2019;70:1317–35.
61. Chazouilleres O. Novel aspects in the management of cholestatic liver diseases. *Dig Dis.* 2016;34:340–6.
62. Zou T, Jaladanki SK, Liu L, Xiao L, Chung HK, Wang JY, Xu Y, et al. H19 long noncoding RNA regulates intestinal epithelial barrier function via MicroRNA 675 by interacting with RNA-binding protein HuR. *Mol Cell Biol.* 2016;36:1332–41.
63. Yu TX, Chung HK, Xiao L, Piao JJ, Lan S, Jaladanki SK, Turner DJ, et al. Long noncoding RNA H19 impairs the intestinal barrier by suppressing autophagy and lowering paneth and goblet cell function. *Cell Mol Gastroenterol Hepatol.* 2020;9:611–25.
64. Gu S, Cao B, Sun R, Tang Y, Paletta JL, Wu X, Liu L, et al. A metabolomic and pharmacokinetic study on the mechanism underlying the lipid-lowering effect of orally administered berberine. *Mol Biosyst.* 2015;11:463–74.
65. Jones BV, Begley M, Hill C, Gahan CG, Marchesi JR. Functional and comparative metagenomic analysis of bile salt hydrolase activity in the human gut microbiome. *Proc Natl Acad Sci USA.* 2008;105:13580–5.
66. Li Y, Tang R, Leung PSC, Gershwin ME, Ma X. Bile acids and intestinal microbiota in autoimmune cholestatic liver diseases. *Autoimmun Rev.* 2017;16:885–96.

Publisher's Note

Springer Nature remains neutral with regard to jurisdictional claims in published maps and institutional affiliations.